IOP Publishing Journal of Physics A: Mathematical and Theoretical
J. Phys. A: Math. Theor. **55** (2022) 274003 (33pp) https://doi.org/10.1088/1751-8121/ac72d7

Local order metrics for two-phase media across length scales*

Salvatore Torquato[1,2,**], **Murray Skolnick**[3] **and Jaeuk Kim**[4]

[1] Department of Chemistry, Department of Physics, Princeton Institute for the Science and Technology of Materials, Program in Applied and Computational Mathematics, Princeton University, Princeton, New Jersey 08544, United States of America
[2] School of Natural Sciences, The Institute for Advanced Study, Princeton, New Jersey 08540, United States of America
[3] Department of Chemistry, Princeton University, Princeton, New Jersey 08544, United States of America
[4] McKetta Department of Chemical Engineering, University of Texas at Austin, Austin, Texas 78712, United States of America

E-mail: torquato@princeton.edu

Received 31 January 2022, revised 14 May 2022
Accepted for publication 24 May 2022
Published 7 July 2022

Abstract

The capacity to devise order metrics to characterize and classify microstructures of multiphase heterogeneous media across length scales is an outstanding but highly challenging task, given the richness of the possible geometries and topologies of the phases that can arise. This investigation initiates a program to formulate order metrics to characterize the degree of order/disorder of the microstructures of two-phase media in d-dimensional Euclidean space $\mathbb{R}^d$ across length scales. In particular, we propose the use of the local volume-fraction variance $\sigma_V^2(R)$ associated with a spherical window of radius R as an order metric. We determine $\sigma_V^2(R)$ as a function of R for 22 different models across the first three space dimensions, including both hyperuniform and non-hyperuniform systems with varying degrees of short- and long-range order. We find that the local volume-fraction variance as well as asymptotic coefficients and integral measures derived from it provide reasonably robust and sensitive order metrics to categorize disordered and ordered two-phase media across all

*Dedicated to Robert M Ziff on the occasion of his 70th birthday.
**Author to whom any correspondences should be addressed.

length scales. Such order metrics could be employed to accelerate the discovery of novel heterogeneous materials by tailoring their degree of order/disorder.

Keywords: length scales, order metrics, two-phase media, hyperuniformity

(Some figures may appear in colour only in the online journal)

1. Introduction

Heterogeneous multiphase media and materials abound in nature and synthetic situations. Examples of such materials include composites, porous media, foams, cellular solids, colloidal suspensions, granular media, polymer blends, geological media, and biological media [1–5]. It is known that the effective transport, mechanical and electromagnetic properties of heterogeneous media depend in a nontrivial manner on the microstructures and phase constituents [2, 4, 6, 7]. Given the multitude of possible microstructures of varying geometries and topologies, it is highly desirable to devise scalar order metrics to characterize the degree of order/disorder of the microstructures. While the study of scalar order metrics to characterize the degree of order/disorder of point configurations has been a fruitful endeavor [8], it is much more challenging to devise such order metrics to describe the microstructures of multiphase media for two reasons. First, the geometries and topologies of the phases are generally much richer and more complex than those of point-configuration arrangements. Second, one must determine characteristic microscopic length scales that are broadly applicable for the plethora of possible microstructures. The capacity to identify useful order metrics for multiphase media could accelerate materials discovery. For example, if sensitive order metrics can be established, one can then formulate experimental or numerical protocols that generate multiphase microstructures with prescribed order metrics and desirable physical properties [9]. This process could be accelerated via machine learning [10–12] by incorporating order metrics to score microstructure data sets.

This paper initiates a program to formulate order metrics to characterize the degree of order/disorder of the microstructures of *two-phase* media in d-dimensional Euclidean space $\mathbb{R}^d$ across length scales. In particular, we propose the use of various measures of volume-fraction fluctuations within a d-dimensional spherical window of radius R as order metrics. Such fluctuations are known to be of importance in a variety of problems, including the study of noise and granularity of photographic images [13, 14], transport through composites and porous media [15], the properties of organic coatings [16], the fracture of composite materials [17], and the scattering of waves in heterogeneous media [18–20].

For concreteness, we focus on two-phase media in $\mathbb{R}^d$ in this work, but we note that the generalization of our results to n-phase media is straightforward. The global volume fractions of phases 1 and 2 are denoted by ϕ_1 and ϕ_2, respectively, where $\phi_1 + \phi_2 = 1$. At a local level, the phase volume fraction fluctuates. The simplest measure of volume-fraction fluctuations is the *local volume-fraction variance* $\sigma_V^2(R)$ (see figure 1), which can be expressed in terms of the autocovariance function $\chi_V(\mathbf{r})$ [21, 22] (defined in section 2):

$$\sigma_V^2(R) = \frac{1}{v_1(R)} \int_{\mathbb{R}^d} \chi_V(\mathbf{r})\, \alpha_2(r; R) \mathrm{d}\mathbf{r}, \tag{1}$$

where

$$v_1(R) = \frac{\pi^{d/2} R^d}{\Gamma(d/2 + 1)} \tag{2}$$

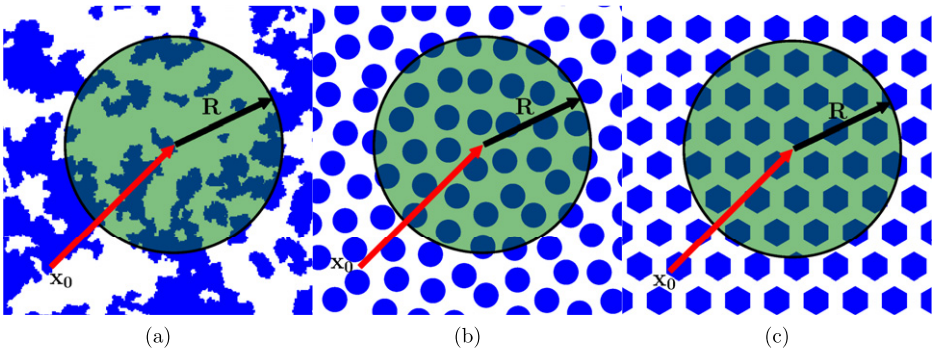

Figure 1. Schematics indicating a circular observation window of radius R in two dimensions, and its centroid $\mathbf{x}_0$ for three different two-phase microstructures: (a) a general disordered nonhyperuniform medium; (b) a disordered hyperuniform medium; and (c) an ordered (periodic) medium. Reprinted from [24], Copyright (2018), with permission from Elsevier. In each of these examples, the phase volume fraction within a window fluctuates as the window centroid varies. While the local variance $\sigma_V^2(R)$ for the nonhyperuniform medium decays like $1/R^2$, it decays like $1/R^3$ in both the disordered hyperuniform and periodic examples.

is the volume of a d-dimensional sphere of radius R, $\Gamma(x)$ is the gamma function and $\alpha_2(r;R)$ is the intersection volume of two spherical windows of radius R separated by a distance r divided by the volume of a window. The quantity $\alpha_2(r;R)$ is known analytically in any space dimension [23]. Note that $\sigma_V^2(R=0)=\phi_1\phi_2$ [21], which can be proved to be an upper bound on the local variance, i.e., $\sigma_V^2(R)\leqslant\phi_1\phi_2$ for all R. In addition to the direct-space representation (1), the local variance $\sigma_V^2(R)$ has the following Fourier-space representation in terms of the spectral density $\tilde{\chi}_V(k)$ [22, 24]:

$$\sigma_V^2(R)=\frac{1}{v_1(R)\,(2\pi)^d}\int_{\mathbb{R}^d}\tilde{\chi}_V(\mathbf{k})\,\tilde{\alpha}_2(k;R)\,\mathrm{d}\mathbf{k}, \tag{3}$$

where $\mathbf{k}$ is the wavevector, $k\equiv|\mathbf{k}|$ is the wavenumber,

$$\tilde{\alpha}_2(k;R)\equiv 2^d\pi^{d/2}\,\Gamma\big(d/2+1\big)\,\frac{[J_{d/2}(kR)]^2}{k^d} \tag{4}$$

is the Fourier transform of $\alpha_2(r;R)$ [25], and $J_\nu(x)$ is the Bessel function of the first kind of order ν (see section 4.10 for plots of $\tilde{\alpha}_2(k;R)$ for $d=1,2$, and 3). The spectral density $\tilde{\chi}_V(\mathbf{k})$ is the Fourier transform of the autocovariance function $\chi_V(\mathbf{r})$ and is directly related to the scattering intensity [26].

The large-R behavior of $\sigma_V^2(R)$ is at the heart of the hyperuniformity concept. Hyperuniform two-phase media are characterized by an anomalous suppression of volume-fraction fluctuations relative to garden-variety disordered media [22, 24] and can be endowed with novel properties [9, 19, 24, 27–41]. Specifically, a hyperuniform two-phase system is one in which $\sigma_V^2(R)$ decays faster than R^{-d} in the large-R regime [22, 24], i.e.,

$$\lim_{R\to\infty}R^d\,\sigma_V^2(R)=0. \tag{5}$$

Equivalently, a hyperuniform medium is one in which the *spectral density* $\tilde{\chi}_V(\mathbf{k})$ goes to zero as $|\mathbf{k}|$ tends to zero [22, 24], i.e.,

$$\lim_{|\mathbf{k}|\to 0} \tilde{\chi}_V(\mathbf{k}) = 0. \tag{6}$$

The hyperuniformity concept has led to a unified means to classify equilibrium and nonequilibrium states of matter, whether hyperuniform or not, according to their large-scale fluctuation characteristics. Suppose the spectral density has the following power-law behavior as $|\mathbf{k}|$ tends to zero:

$$\tilde{\chi}_V(\mathbf{k}) \sim |\mathbf{k}|^{\alpha} \quad (|\mathbf{k}| \to 0), \tag{7}$$

where α is an exponent that specifies whether the medium is hyperuniform or not. In the case of hyperuniform two-phase media, $\alpha > 0$, and it has been shown [22, 24] that there are three different scaling regimes (classes) that describe the associated large-R behaviors of the volume-fraction variance

$$\sigma_V^2(R) \sim \begin{cases} R^{-(d+1)}, & \alpha > 1 \qquad \text{(Class I)} \\ R^{-(d+1)} \ln R, & \alpha = 1 \qquad \text{(Class II)} \\ R^{-(d+\alpha)}, & 0 < \alpha < 1 \qquad \text{(Class III).} \end{cases} \tag{8}$$

Classes I and III are the strongest and weakest forms of hyperuniformity, respectively. Class I media include all crystal structures, many quasicrystal structures and exotic disordered media [22, 24, 42]. Such scalings are due to the fact that the autocovariance function $\chi_V(\mathbf{r})$ decays like $|\mathbf{r}|^{-(d+\alpha)}$ in the large-$\mathbf{r}$ regime for hyperuniform media. For class II and III systems, this rate of decay is slow enough to affect the scaling of the variance. However, for class I systems, the decay rate $|\mathbf{r}|^{-(d+\alpha)}$ is fast enough for the variance to be independent of α [24].

By contrast, for any nonhyperuniform two-phase system, it is straightforward to show, using a similar analysis as for point configurations [43], that the local variance has the following large-R scaling behaviors:

$$\sigma_V^2(R) \sim \begin{cases} R^{-d}, & \alpha = 0 \quad \text{(typical nonhyperuniform)} \\ R^{-(d+\alpha)}, & -d < \alpha < 0 \quad \text{(antihyperuniform).} \end{cases} \tag{9}$$

For a 'typical' nonhyperuniform system, $\tilde{\chi}_V(0)$ is bounded [24]. For *antihyperuniform* media, $\tilde{\chi}_V(0)$ is unbounded, i.e.,

$$\lim_{|\mathbf{k}|\to 0} \tilde{\chi}_V(\mathbf{k}) = +\infty, \tag{10}$$

and hence are diametrically opposite to hyperuniform systems. Antihyperuniform media include systems at thermal critical points (e.g., liquid-vapor and magnetic critical points) [44, 45], fractals [46], disordered non-fractals [47], and certain substitution tilings [48].

In this paper, we propose the use of the local volume-fraction variance $\sigma_V^2(R)$ as an order metric for disordered and ordered two-phase media across all length scales by tracking it as a function of R. Specifically, for any particular value of R, the lower (higher) the volume-fraction fluctuations as measured by $\sigma_V^2(R)$, the greater the degree of order (disorder). We study this order metric and integral measures derived from it across length scales for 22 different models across the first three space dimensions, including both hyperuniform and nonhyperuniform systems with varying degrees of short- and long-range order. Examination of the same model across dimensions enables us to study the effect of dimensionality on the ranking of order across dimensions. For almost all one-dimensional (1D) models and some two-dimensional (2D) and three-dimensional (3D) models, we obtain exact closed-form formulas for their pair statistics and local variances. We find that the local volume-fraction fluctuations, as measured

by the magnitude of $\sigma_V^2(R)$ for a particular value of the window radius R, provide a reasonably robust way to rank order different two-phase media at a common global volume fraction. We also calculate the implied coefficients multiplying the large-R scaling of the variance for class I hyperuniform media [cf (8)] and that of typical nonhyperuniform media [cf (9)]. The calculation of such large-R asymptotic coefficients was only recently carried out, but primarily for certain 2D ordered structures [49].

In section 2, we present necessary definitions and background material. In section 3, we derive a useful Fourier-space representation of a large-R asymptotic coefficient that we employ in subsequent sections. Brief descriptions of the two-phase models across the first three space dimensions and their corresponding relevant structural characteristics are given in section 4. In section 5, we present the local variance as well as integral measures derived from it as order metrics. In section 6, we present the major results for the local variance for all of the models. Finally, we make concluding remarks in section 7.

2. Definitions and background

2.1. Correlation functions

A two-phase medium is fully statistically characterized by the n-point correlation functions [2], defined by

$$S_n^{(i)}(\mathbf{x}_1, \ldots, \mathbf{x}_n) \equiv \left\langle \mathcal{I}^{(i)}(\mathbf{x}_1) \ldots \mathcal{I}^{(i)}(\mathbf{x}_n) \right\rangle, \tag{11}$$

where $\mathcal{I}^{(i)}(\mathbf{x})$ is the *indicator function* for phase $i = 1, 2$, defined as

$$\mathcal{I}^{(i)}(\mathbf{x}) \equiv \begin{cases} 1, & \mathbf{x} \text{ in phase } i \\ 0, & \text{otherwise,} \end{cases} \tag{12}$$

where $n = 1, 2, 3, ...$, [50] and angular brackets denote an ensemble average. The function $S_n^{(i)}(\mathbf{x}_1, \ldots, \mathbf{x}_n)$ also has a probabilistic interpretation, namely, it is the probability that the n positions $\mathbf{x}_1, \ldots, \mathbf{x}_n$ all lie in phase i. For statistically homogeneous media, $S_n^{(i)}(\mathbf{x}_1, \ldots, \mathbf{x}_n)$ is translationally invariant and hence depends only on the relative displacements of the points.

The *autocovariance* function $\chi_V(\mathbf{r})$, which is directly related to the two-point function $S_2^{(i)}(\mathbf{r})$ and plays a central role in this paper, is defined by

$$\chi_V(\mathbf{r}) \equiv S_2^{(1)}(\mathbf{r}) - \phi_1^2 = S_2^{(2)}(\mathbf{r}) - \phi_2^2, \tag{13}$$

where $\mathbf{r} \equiv \mathbf{x}_2 - \mathbf{x}_1$. Here, we have assumed statistical homogeneity. The equality in (13) comes from the fact that for two-phase media, $\mathcal{I}^{(1)}(\mathbf{x}) = 1 - \mathcal{I}^{(2)}(\mathbf{x})$. At the extreme limits of its argument, $\chi_V(\mathbf{r})$ has the following asymptotic behavior: $\chi_V(\mathbf{r} = \mathbf{0}) = \phi_1\phi_2$ and $\lim_{|\mathbf{r}|\to\infty} \chi_V(\mathbf{r}) = 0$ if the medium possesses no long-range order. If the medium is statistically homogeneous and isotropic, then the autocovariance function $\chi_V(\mathbf{r})$ depends only on the magnitude of its argument $r = |\mathbf{r}|$, and hence is a radial function. In such instances, its slope at the origin is directly related to the *specific surface* s, which is the interface area per unit volume. In particular, the well-known 3D asymptotic result [26] is easily obtained in any space dimension d:

$$\chi_V(\mathbf{r}) = \phi_1\phi_2 - \kappa(d)s\,|\mathbf{r}| + \mathcal{O}(|\mathbf{r}|^2), \tag{14}$$

where

$$\kappa(d) = \frac{\Gamma(d/2)}{2\sqrt{\pi}\Gamma((d+1)/2)}. \tag{15}$$

The nonnegative spectral density $\tilde{\chi}_V(\mathbf{k})$, which can be obtained from scattering experiments [26, 51], is the Fourier transform of a well-defined integrable autocovariance function $\chi_V(\mathbf{r})$ [52, 53] at wavevector $\mathbf{k}$, i.e.,

$$\tilde{\chi}_V(\mathbf{k}) = \int_{\mathbb{R}^d} \chi_V(\mathbf{r}) \mathrm{e}^{-\mathrm{i}\mathbf{k}\cdot\mathbf{r}} \mathrm{d}\mathbf{r} \geqslant 0, \quad \text{for all } \mathbf{k}. \tag{16}$$

For a general statistically homogeneous two-phase medium, the spectral density must obey the following sum rule [15]:

$$\frac{1}{(2\pi)^d} \int_{\mathbb{R}^d} \tilde{\chi}_V(\mathbf{k})\, \mathrm{d}\mathbf{k} = \chi_V(\mathbf{r} = 0) = \phi_1 \phi_2. \tag{17}$$

For statistically isotropic media, the spectral density only depends on the wavenumber $k = |\mathbf{k}|$ and, as a consequence of (14), its decay in the large-k limit is controlled by the exact following power-law form:

$$\tilde{\chi}_V(k) \sim \frac{\gamma(d)\, s}{k^{d+1}}, \quad k \to \infty, \tag{18}$$

where

$$\gamma(d) = 2^d\, \pi^{(d-1)/2}\, \Gamma((d+1)/2). \tag{19}$$

In the case of a packing of identical particles (nonoverlapping particles) $\mathcal{P}$ of volume $v_1(\mathcal{P})$ at number density ρ, the spectral density $\tilde{\chi}_V(\mathbf{k})$ is directly related to the structure factor $S(\mathbf{k})$ of the particle centroids [2, 24, 42]:

$$\tilde{\chi}_V(\mathbf{k}) = \phi_2 \frac{|\tilde{m}(\mathbf{k}; \mathcal{P})|^2}{v_1(\mathcal{P})} S(\mathbf{k}), \tag{20}$$

where $\tilde{m}(\mathbf{k}; \mathcal{P})$, called the *form factor*, is the Fourier transform of the particle indicator function so that $\tilde{m}(0; \mathcal{P}) = v_1(\mathcal{P})$, and

$$\phi_2 = \rho v_1(\mathcal{P}) \tag{21}$$

is the packing fraction, i.e., the fraction of space covered by the identical nonoverlapping particles. For example, in the case of identical d-dimensional spheres of radius a, the form factor is given by

$$\tilde{m}(k; a) = \left(\frac{2\pi a}{k}\right)^{d/2} J_{d/2}(ka). \tag{22}$$

For any such sphere packing, the specific surface s is given by

$$s = \frac{\phi_2\, d}{a}. \tag{23}$$

Stealthy hyperuniform media are a subclass of hyperuniform media that belong to class I. They are defined to possess zero-scattering intensity for a set of wavevectors around the origin [42], i.e.,

$$\tilde{\chi}_V(\mathbf{k}) = 0 \quad \text{for } 0 \leqslant |\mathbf{k}| \leqslant K. \tag{24}$$

Examples of such media are periodic packings of spheres, unusual disordered sphere packings derived from stealthy point patterns, as well as specially designed stealthy hyperuniform dispersions [42, 54, 55].

2.2. Large-R asymptotic analysis of the variance

For a large class of statistically homogeneous two-phase media in $\mathbb{R}^d$, the large-R asymptotic expansion of the local volume-fraction variance $\sigma_V^2(R)$ is given by [22]:

$$\sigma_V^2(R) = \bar{A}_V\left(\frac{D}{R}\right)^d + \bar{B}_V\left(\frac{D}{R}\right)^{d+1} + o\left(\frac{D}{R}\right)^{d+1}, \tag{25}$$

where $\bar{A}_V$ and $\bar{B}_V$ are dimensionless asymptotic coefficients of powers R^{-d} and $R^{-(d+1)}$, respectively, given by

$$\bar{A}_V = \frac{1}{v_1(D)}\int_{\mathbb{R}^d}\chi_V(\mathbf{r})\,\mathrm{d}\mathbf{r} = \frac{\tilde{\chi}_V(\mathbf{k}=\mathbf{0})}{v_1(D)}, \tag{26}$$

$$\bar{B}_V = -\frac{c(d)}{2Dv_1(D)}\int_{\mathbb{R}^d}\chi_V(\mathbf{r})\,|\mathbf{r}|\mathrm{d}\mathbf{r}, \tag{27}$$

where $c\,(d) \equiv 2\Gamma\big(1+d/2\big)\,/[\pi^{1/2}\Gamma\big((d+1)/2\big)]D$ is a characteristic microscopic length scale of the medium, and $o\big(D/R\big)^{d+1}$ represents terms of order higher than $\big(D/R\big)^{d+1}$. For typical nonhyperuniform media, $\bar{A}_V$ is positive [cf (9)]. When $\bar{A}_V = 0$, $\bar{B}_V$ must be positive, implying that the medium is hyperuniform of class I [cf (8)]. It is noteworthy that, unlike $\sigma_V^2(R)$, the coefficient $\bar{B}_V$ depends on the choice of the length scale D. Appendix A provides a more general asymptotic expansion of the local volume-fraction variance. Finally, we note that for any packing of identical particles, formulas (20) and (26) yield the leading-order asymptotic coefficient to be generally given by

$$\bar{A}_V = \phi_2 S(0), \tag{28}$$

which was first derived in reference [22].

3. Fourier-space representation of the asymptotic coefficient $\bar{B}_V$

Here we derive a Fourier-space representation of the asymptotic coefficient $\bar{B}_V$ for any homogeneous two-phase system, whether hyperuniform or not, provided that the spectral density meets certain mild conditions. This representation will be especially useful when the scattering intensity is available experimentally or if the spectral density is known analytically. Specifically, the coefficient $\bar{B}_V$ can be expressed as follows:

$$\bar{B}_V = \frac{\Gamma(1+d/2)d}{\pi^{(d+2)/2}D^{d+1}}\int_0^\infty \frac{\tilde{\chi}_V(k)-\tilde{\chi}_V(0)}{k^2}\,\mathrm{d}k, \tag{29}$$

where $\tilde{\chi}_V(0) \equiv \lim_{|\mathbf{k}|\to 0}\tilde{\chi}_V(\mathbf{k})$. This Fourier representation of the coefficient $\bar{B}_V$ is the analog of the one derived for point configurations [43]. Thus, this Fourier-space representation of the coefficient $\bar{B}_V$ is bounded provided that the difference $[\tilde{\chi}_V(k)-\tilde{\chi}_V(0)]$ tends to zero in the limit $k\to 0$ faster than linear in k. This condition will always be met by any spectral density that is analytic at the origin, since $[\tilde{\chi}_V(k)-\tilde{\chi}_V(0)]$ must vanish at least as fast as quadratically in k as $k\to 0$. In this paper, we will often use formula (29) to determine $\bar{B}_V$, either analytically or numerically.

To prove the formula (29), we begin by using the identity [25]

$$\frac{1}{(2\pi)^d}\int_{\mathbb{R}^d}\tilde{\alpha}_2(k;R)\mathrm{d}\mathbf{k} = 1, \tag{30}$$

in relation (3) to yield

$$\sigma_V^2(R) = \frac{\tilde{\chi}_V(0)}{v_1(R)} + \frac{1}{v_1(R)(2\pi)^d}\int_{\mathbb{R}^d}[\tilde{\chi}_V(\mathbf{k}) - \tilde{\chi}_V(0)]\tilde{\alpha}_2(k;R)\mathrm{d}\mathbf{k}. \tag{31}$$

Since $\tilde{\alpha}_2(k;R)$ is a radial function, depending only on the magnitude of the wavevector, we can carry out the angular integration in the integral in (31), yielding

$$\sigma_V^2(R) = \frac{\tilde{\chi}_V(0)}{v_1(R)} + \frac{d}{R^d(2\pi)^d}\int_0^\infty k^{d-1}[\tilde{\chi}_V(k) - \tilde{\chi}_V(0)]\tilde{\alpha}_2(k;R)\mathrm{d}k, \tag{32}$$

where the radial function $\tilde{\chi}_V(k)$ is given by

$$\tilde{\chi}_V(k) = \frac{1}{\Omega}\int_\Omega \tilde{\chi}_V(\mathbf{k})\mathrm{d}\Omega, \tag{33}$$

where $\mathrm{d}\Omega$ is the differential solid angle and $\Omega = \frac{d\pi^{d/2}}{\Gamma(1+d/2)}$ is the total solid angle contained in a d-dimensional sphere. For large R,

$$\tilde{\alpha}_2(k;R) \sim 2^{d+1}\pi^{d/2-1}\Gamma(1+d/2)\frac{\cos^2\left[kR - \frac{d+1}{4}\right]}{Rk^{d+1}}. \tag{34}$$

Combination of (32) and (34) yields the following large-R asymptotic expansion:

$$\sigma_V^2(R) \sim \frac{\tilde{\chi}_V(0)}{v_1(R)} + \frac{2\Gamma(1+d/2)\,d}{R^{d+1}\pi^{(d+2)/2}} \times \int_0^\infty \frac{[\tilde{\chi}_V(k) - \tilde{\chi}_V(0)]}{k^2}\cos^2\left[kR - \frac{d+1}{4}\right]\mathrm{d}k + \mathcal{O}\left(\frac{1}{R^{d+3}}\right). \tag{35}$$

Using the identity

$$\lim_{L\to\infty}\frac{1}{L}\int_0^L \cos^2\left[kR - \frac{d+1}{4}\right]\mathrm{d}R = \frac{1}{2} \tag{36}$$

and (35), we obtain

$$\sigma_V^2(R) \sim \frac{\tilde{\chi}_V(0)}{v_1(R)} + \frac{\Gamma(1+d/2)\,d}{R^{d+1}\pi^{(d+2)/2}}\int_0^\infty \frac{[\tilde{\chi}_V(k) - \tilde{\chi}_V(0)]}{k^2}\mathrm{d}k + \mathcal{O}\left(\frac{1}{R^{d+3}}\right). \tag{37}$$

Comparing (37) to (25) yields the desired Fourier-space representation of the surface-area coefficient $\bar{B}_V$ given by (29). Finally, we observe that if the coefficient $\bar{B}_V$ is identically zero, relation (29) leads to the integral condition

$$\int_0^\infty \frac{\tilde{\chi}_V(k) - \tilde{\chi}_V(0)}{k^2}\mathrm{d}k = 0, \tag{38}$$

which is the analog of the Fourier-space sum rule for *hyposurficial* point configurations [25].

4. Two-phase media models

4.1. Antihyperuniform media

We consider the following autocovariance function corresponding to a model of antihyperuniform media in three dimensions devised by Torquato [47]:

$$\frac{\chi_V(r)}{\phi_1\phi_2} = \frac{1}{1 + 2(r/a) + (r/a)^2}, \tag{39}$$

whose specific surface is given by

$$s = \frac{8\phi_1\phi_2}{a}. \tag{40}$$

This monotonic functional form meets all of the known necessary realizability conditions on a valid autocovariance function [42]. The corresponding spectral density is given by

$$\tilde{\chi}_V(k) = \frac{4\pi a^2}{ka}\left\{\mathrm{Ci}(ka)[ka\,\cos(ka) + \sin(ka)] + \mathrm{Ssi}(ka)\,[ka\,\sin(ka) - \cos(ka)\right\}, \tag{41}$$

where $\mathrm{Ci}(x) \equiv \int_0^x \mathrm{d}t\,\cos(t)/t$ is the cosine integral, $\mathrm{Ssi}(x) \equiv \mathrm{Si}(x) - \pi/2$ is the shifted sine integral and $\mathrm{Si}(x) \equiv \int_0^x \mathrm{d}t\,\sin(t)/t$ is the sine integral. We see that $\tilde{\chi}_V(k) \sim 2\pi^2/k$ in the limit $k \to 0$, which is consistent with the power-law decay $1/r^2$ of $\chi_V(r)$ in the limit $r \to \infty$.

4.2. Debye random media

Debye *et al* [26] hypothesized that the following autocovariance function characterizes isotropic random media in which the phases form domains of 'random shape and size':

$$\chi_V(r) = \phi_1\phi_2\,\exp(-r/a), \tag{42}$$

where a is a characteristic length scale. The Taylor expansion of (42) about $r = 0$ and comparison to (14) reveals that the specific surface s of a Debye random medium in any space dimension is given by

$$s = \frac{\phi_1\,\phi_2}{\kappa(d)\,a}. \tag{43}$$

The spectral density for Debye random media in any space dimension is given by [15]

$$\tilde{\chi}_V(k) = \frac{\phi_1\phi_2\,c_d\,a^d}{[1 + (ka)^2]^{(d+1)/2}}, \tag{44}$$

where $c_d = 2^d\pi^{(d-1)/2}\Gamma((d+1)/2)$.

4.3. Overlapping spheres

The model of overlapping spheres or fully-penetrable-sphere model refers to an uncorrelated (Poisson) distribution of spheres of radius a throughout a matrix [2]. For such nonhyperuniform models at number density in d-dimensional Euclidean space $\mathbb{R}^d$, the autocovariance function is known analytically [2]:

$$\chi_V(r) = \exp(-\rho v_2(r;a)) - {\phi_1}^2, \tag{45}$$

where $\phi_1 = \exp(-\rho v_1(a))$ is the volume fraction of the matrix phase (phase 1), $v_1(a)$ is given by (2), and $v_2(r;a)$ represents the union volume of two spheres whose centers are separated by a distance r. In two and three dimensions, the latter is explicitly given respectively by

$$\frac{v_2(r;a)}{v_1(a)} = \begin{cases} 2\Theta(x-1) + (1+x)\Theta(1-x), & d=1 \\ 2\Theta(x-1) + \dfrac{2}{\pi}\left[\pi + x(1-x^2)^{1/2} - \cos^{-1}(x)\right]\Theta(1-x), & d=2 \\ 2\Theta(x-1) + \left(1 + \dfrac{3x}{2} - \dfrac{x^3}{2}\right)\Theta(1-x), & d=3, \end{cases} \tag{46}$$

where $x \equiv r/2a$, and $\Theta(x)$ (equal to 1 for and zero otherwise) is the Heaviside step function. The specific surface s in any space dimension is given by [2]

$$s = \frac{\eta\phi_1 d}{a}, \tag{47}$$

where $\eta \equiv \rho v_1(a)$. For $d = 1$, the spectral density can be expressed in the following closed-form:

$$\tilde{\chi}_V(k) = \frac{2\phi_1\eta}{k((2ak)^2 + \eta^2)}\left[2ak(1 - \phi_1\cos(2ak)) + \phi_1\eta\sin(2ak)\right]. \tag{48}$$

4.4. Random checkerboard

The random checkerboard in d dimensions is generated by tessellating space into identical hypercubic cells of side length a and randomly designating a cell as phase 1 or 2 with probability ϕ_1 or ϕ_2, respectively. The angular-averaged autocovariance takes the form [2]

$$\chi_V(r) = W(r)\phi_1\phi_2, \tag{49}$$

where $W(r)$ is a radial function with support in the interval $[0, \sqrt{d}\,a]$. For example, for $d = 1$,

$$W(r) = (1-x)\Theta(1-x),$$

and for $d = 2$,

$$W(r) = \begin{cases} 1 + \dfrac{x^2 - 4x}{\pi}, & 0 \leqslant x \leqslant 1 \\ 1 - \dfrac{2+x^2}{\pi} + \dfrac{4}{\pi}\left[(x^2-1)^{1/2} - \cos^{-1}\left(1/x\right)\right], & 1 \leqslant x \leqslant \sqrt{2} \\ 0, & x \geqslant \sqrt{2}, \end{cases} \tag{50}$$

where $x = r/a$. The explicit expression for $W(r)$ for $d = 3$ is given in reference [2]. The specific surface s in any space dimension is given by [2]

$$s = \frac{2d\,\phi_1\phi_2}{a}. \tag{51}$$

For $d = 1$, the spectral density can be expressed in the following closed-form:

$$\tilde{\chi}_V(k) = \phi_1\phi_2 a\frac{\sin^2(ka/2)}{(ka/2)^2}. \tag{52}$$

4.5. Equilibrium packings

We also examine equilibrium (Gibbs) ensembles of identical hard spheres of radius a at packing fraction ϕ_2 [8, 56]. In particular, we consider such disordered packings along the stable disordered fluid branch in the phase diagram [2, 8]. All such states are nonhyperuniform. In the case of 1D equilibrium hard rods, pair statistics are known exactly [57]. In particular, using the exact solution of the direct correlation function [57, 58] and the Ornstein–Zernike integral equation, we can express the exact structure factor as

$$S(k) = \left[1 - \frac{2\phi_2\left\{\phi_2\left[\cos(2ak) - 1\right] + 2ak\,\sin(2ak)(\phi_2 - 1)\right\}}{(1-\phi_2)^2(2ak)^2}\right]^{-1}.$$

For $d = 3$, we utilize the Percus–Yevick approximation of the structure factor $S(k)$ [56]:

$$S(k) = \left(1 - \rho\frac{16\pi a^3}{q^6}\left\{\left[24a_1\phi_2 - 12(a_1 + 2a_2)\phi_2 q^2 + (12a_2\phi_2 + 2a_1 + a_2\phi_2)q^4\right]\cos(q)\right.\right.$$
$$\left.\left. + \left[24a_1\phi_2 q - 2(a_1 + 2a_1\phi_2 + 12a_2\phi_2)q^3\right]\sin(q) - 24\phi_2(a_1 - a_2q^2)\right\}\right)^{-1},$$

where $q = 2ka$, $a_1 = (1 + 2\phi_2)^2/(1-\phi_2)^4$, and $a_2 = -(1 + \phi_2/2)^2/(1-\phi_2)^4$. Using these solutions for the structure factor in conjunction with (20) yields the corresponding spectral density $\tilde{\chi}_V(k)$. For $d = 2$, there is no closed-form approximation for the structure, and so we obtain the spectral density from disk packings generated by the Monte Carlo method [2].

4.6. Disordered hyperuniform media

We also consider models of hyperuniform two-phase media in $\mathbb{R}^d$ formulated by Torquato [42, 59] in which the autocovariance function takes the following form:

$$\frac{\chi_V(r)}{\phi_1\phi_2} = c\,\mathrm{e}^{-r/a}\,\cos(qr + \theta), \tag{54}$$

where the parameters q and θ are the wavenumber and phase associated with the oscillations of $\chi_V(r)$, respectively, a is a correlation length, and c is a normalization constant to be chosen so that the right-hand side of (54) is unity for $r = 0$. For $d = 1$, the phase is given by $\theta = \tan^{-1}\big(1/(qa)\big)$, implying that the normalization constant is $c = [1 + (qa)^2]^{1/2}/(qa)$. For concreteness, we set $qa = 1$, and hence $c = \sqrt{2}$ and $\theta = \pi/4$. Taking the Fourier transform of (54) with these parameters yields the spectral density to be given by

$$\frac{\tilde{\chi}_V(k)}{\phi_1\phi_2} = \frac{4\,(ka)^2\,a}{(ka)^4 + 4}. \tag{55}$$

In higher dimensions, one can take $\theta = 0$ and $c = 1$. The corresponding spectral densities for $d = 2$ with $(qa)^2 = 1$ and $d = 3$ with $(qa)^2 = 1/3$ are respectively given by

$$\frac{\tilde{\chi}_V(k)}{\phi_1\phi_2} = \frac{2\pi(ka)^2[A(k) + B(k)] + 4\pi[A(k) - B(k)]\,a^2}{[(ka)^4 + 4][A^2(k) + B^2(k)]}, \tag{56}$$

and

$$\frac{\tilde{\chi}_V(k)}{\phi_1\phi_2} = \frac{216\pi\,[3(ka)^2 + 8](ka)^2\,a^3}{81(ka)^8 + 216(ka)^6 + 432(ka)^4 + 384(ka)^2 + 256}, \tag{57}$$

where

$$A(k) = \sqrt{(ka)^2/2 + \sqrt{(ka)^4 + 4}/2}, \qquad B(k) = A^{-1}(k). \tag{58}$$

Note that the specific surface s for this system in any dimension d is given by

$$s = \frac{2\sqrt{\pi}c\phi_1\phi_2\Gamma\left[(1+d)/2\right]\left[\cos(\theta) + qa\,\sin(\theta)\right]}{a\Gamma[d/2]}. \tag{59}$$

4.7. Stealthy hyperuniform media

We also study 'stealthy' hyperuniform two-phase media, which obey the general functional form given by (24), where K is the exclusion sphere radius in Fourier (reciprocal) space. One can create stealthy packings of identical spheres by decorating stealthy point configurations, generated via the so-called collective-coordinate optimization technique [60, 61], by spheres of radius a such that spheres cannot overlap [62]. Here we utilize a modification of this algorithm by incorporating an additional soft-core repulsive interaction between the points to further increase the nearest-neighbor distance so that even higher packing fractions can be achieved by a decoration of the points by nonoverlapping spheres [19, 38]. Disordered stealthy point configurations generated by this optimization procedure are actually classical ground states of systems of particles interacting with bounded long-ranged pair potentials. The corresponding spectral densities in this work are obtained from the numerically generated stealthy packings.

4.8. Periodic media

We consider nonoverlapping particles $\mathcal{P}$ on the sites of any Bravais lattice $\mathcal{L}$ in $\mathbb{R}^d$ in which a single particle $\mathcal{P}$ is placed in a fundamental cell $\mathcal{F}$ of $\mathcal{L}$. One can immediately obtain from (20) the specific formulas for the corresponding spectral density as follows:

$$\tilde{\chi}_V(\mathbf{k}) = {V_{\mathcal{F}}}^{-1}|\tilde{m}(\mathbf{k};\mathcal{P})|^2 S_{\mathcal{L}}(\mathbf{k}), \tag{60}$$

where $V_{\mathcal{F}}$ is the volume of $\mathcal{F}$, $S_L(\mathbf{k})$ is the structure factor of $\mathcal{L}$ given by [24]

$$S_{\mathcal{L}}(\mathbf{k}) = \frac{(2\pi)^d}{V_{\mathcal{F}}} \sum_{\mathbf{q}\in\mathcal{L}^*\setminus\{0\}} \delta(\mathbf{k}-\mathbf{q}), \tag{61}$$

where $\mathcal{L}^*$ denotes the reciprocal lattice of $\mathcal{L}$, and $\delta(x)$ is the Dirac delta function. Specifically, for $d = 1$, we consider rods of phase 2 placed on the sites of the integer lattice, whose specific surface is given by (23). For $d = 2$, we consider both circular disks and oriented hexagons of side length a placed on the sites of the triangular lattice, whose specific surfaces are given by (23) and $s = 4\phi_2/(\sqrt{3}a)$, respectively [49]. The form factor $\tilde{m}(k;\mathcal{P})$ for the hexagon is obtained using the analysis presented in reference [49]. For $d = 3$, we consider spheres on the sites of both the simple cubic (SC) and body-centered cubic (BCC) lattices, whose specific surfaces are given by (23).

4.9. Representative microstructure images

To get a visual sense of the breadth of microstructures considered in this paper that span from nonhyperuniform to hyperuniform two-phase media and their corresponding degree of order, we depict representative images of small portions of the microstructures of each of the eight

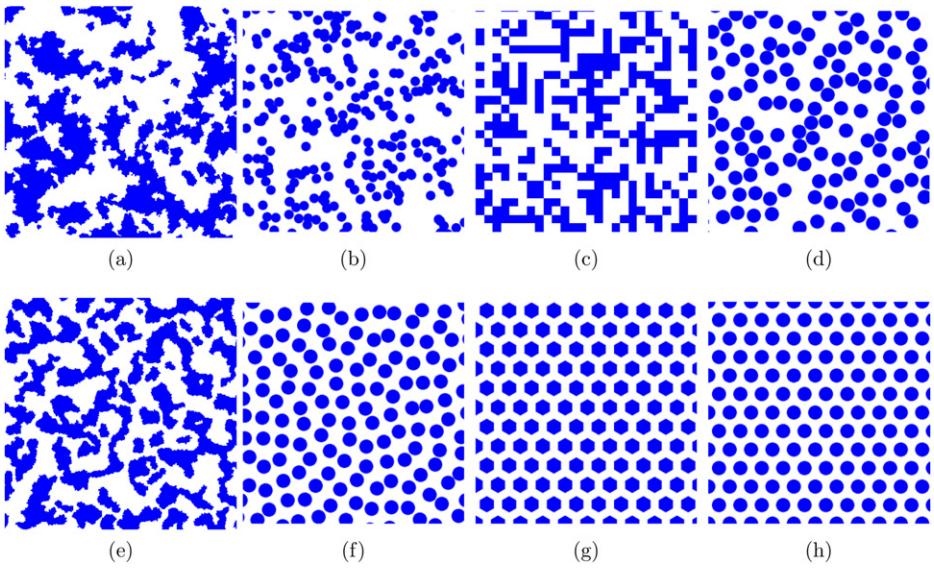

Figure 2. Representative images of each of the eight 2D two-phase models at $\phi_2 = 0.4$: (a) Debye random media; (b) overlapping circular disks; (c) random checkerboard; (d) equilibrium hard disks; (e) disordered hyperuniform; (f) stealthy hyperuniform disks; (g) hexagons on the triangular lattice; (h) circular disks on the triangular lattice. Here, the white regions represent phase 1 and the blue regions represent phase 2.

2D two-phase models at $\phi_2 = 0.4$ in figure 2. It is expected that Debye random media will be the most disordered at all length scales because they are characterized by phase domains of random shapes with a wide range of sizes, including a substantial fraction of large 'holes' [15, 63, 64]. We will see that this expectation is indeed the case in section 6, as well as the fact that circular disks on the triangular lattice are the most ordered.

4.10. Results for the spectral densities

The spectral densities for 1D, 2D and 3D models are depicted in figures 3–5, respectively. According to formula (3) for the local variance $\sigma_V^2(R)$, the behavior of the spectral density for small to intermediate wavenumbers determines the magnitude of the local variance for intermediate to large length scales. In particular, the smaller (larger) are the values of $\tilde{\chi}_V(k)$ for such wavenumbers, the smaller (larger) are the values of $\sigma_V^2(R)$ for intermediate to large length scales. More precisely, we see from formula (3) that it is the product of the spectral density with function $\tilde{\alpha}_2(k;R)$ [cf (4)] that determines the behavior of $\sigma_V^2(R)$. We see from the plots of $\tilde{\alpha}_2(k;R)$ for the first three space dimensions shown in figure 6 that the function (4) places increasingly heavier weight on the small wavenumber region of the spectral density in integral (3) as the dimension increases. Thus, qualitative changes in the spectral densities for the same models across dimensions have implications for how their relative order ranking may or may not change across dimensions. For example, while the dimensionless spectral density for the 1D random checkerboard is substantially smaller than that for equilibrium hard rods for a range of wavenumbers near the origin (figure 3), these behaviors for their 2D counterparts are reversed (figure 3), which, in turn, should reverse their relative rankings, which we will see is indeed the case in section 6. Across dimensions, periodic media are characterized by Bragg peaks (Dirac delta functions) whose strengths are proportional to the form factor [cf (20)]. In

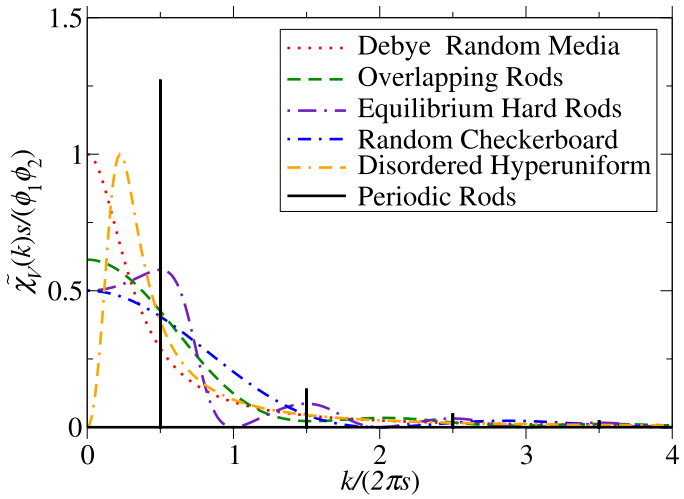

Figure 3. Comparison of the dimensionless spectral densities $\tilde{\chi}_V(k)s/(\phi_1\phi_2)$ versus the dimensionless wavenumber $k/(2\pi s)$ for 1D models at $\phi_2 = 0.5$, where s is the specific surface.

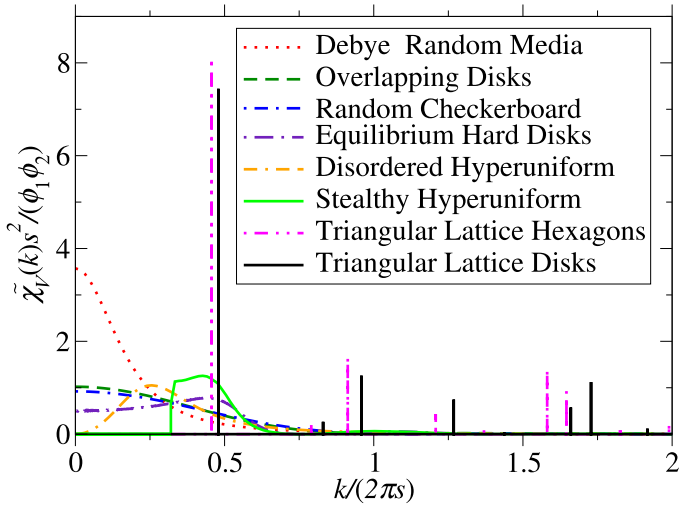

Figure 4. Comparison of the dimensionless spectral densities $\tilde{\chi}_V(k)s^2/(\phi_1\phi_2)$ versus the dimensionless wavenumber $k/(2\pi s)$ for 2D models at, where s is the specific surface. In the case of periodic media, the angular-averaged spectral density is presented.

the 2D and 3D periodic cases, the structures with the largest first Bragg peak (i.e., triangular lattice of circles in 2D and BCC lattice of spheres in 3D) should yield the least fluctuations in those dimensions, which again is verified in section 6. For the same reasons, the stealthy hyperuniform packings in 2D and 3D should yield the most ordered microstructures among all disordered models.

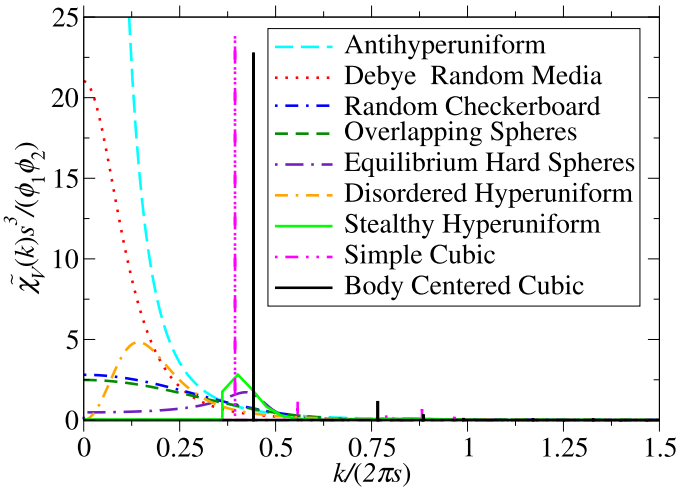

Figure 5. Comparison of the dimensionless spectral densities $\tilde{\chi}_V(k)s^3/(\phi_1\phi_2)$ versus the dimensionless wavenumber $k/(2\pi s)$ for 3D models at $\phi_2 = 0.38$, where s is the specific surface. In the case of periodic media, the angular-averaged spectral density is presented.

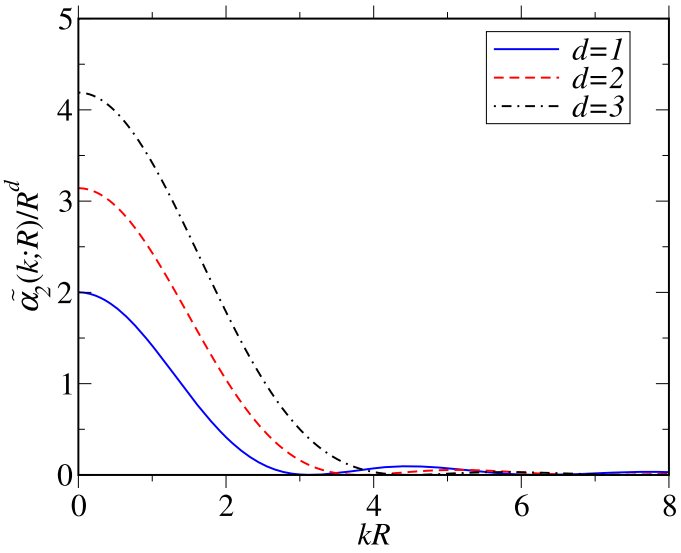

Figure 6. Plots of the Fourier transform of the scaled intersection volume of two spherical windows (4) normalized by R^d, $\tilde{\alpha}_2(k;R)/R^d$, as a function of dimensionless wavevector kR for dimensions one, two, and three. Reprinted from [24], Copyright (2018), with permission from Elsevier.

5. Local variance as an order metric across length scales

We propose the use of the local volume-fraction variance $\sigma_V^2(R)$ at window radius R as an order metric for disordered and ordered two-phase media across length scales by tracking it

as a function of R. Specifically, for any particular value of R, the lower the value of $\sigma_V^2(R)$, the greater the degree of order.

To extract an integrated measure of local volume-fraction fluctuations for window radii from zero to some length scale L, we consider the following 1D integral over $\sigma_V^2(R)$:

$$\Sigma_V(L) = \int_0^L \sigma_V^2(R)\mathrm{d}R. \tag{62}$$

Whenever the integral $\Sigma_V(L)$ converges, i.e., is bounded, in the limit $L \to \infty$, we consider

$$\Sigma_V(\infty) \equiv \int_0^\infty \sigma_V^2(R)\mathrm{d}R. \tag{63}$$

This integral has the following convenient closed-form representation in terms of the angular-averaged spectral density defined by (33):

$$\Sigma_V(\infty) = \frac{\Gamma(1+d/2)\Gamma(d/2)\,d}{2\pi^{d/2}\Gamma(d+1/2)\Gamma((d+1)/2)}\int_0^\infty k^{d-2}\tilde{\chi}_V(k)\mathrm{d}k. \tag{64}$$

To prove relation (64), we substitute formula (3) into (63) to yield

$$\Sigma_V(\infty) = \frac{1}{(2\pi)^d}\int_{\mathbb{R}^d}\tilde{\chi}_V(\mathbf{k})\mathrm{d}\mathbf{k}\int_0^\infty \frac{\tilde{\alpha}_2(k;R)}{v_1(R)}\mathrm{d}R \tag{65}$$

$$= \frac{d}{(2\pi)^d}\int_0^\infty k^{d-1}\tilde{\chi}_V(k)\mathrm{d}k\int_0^\infty \frac{\tilde{\alpha}_2(k;R)}{R^d}\mathrm{d}R \tag{66}$$

$$= \frac{\Gamma(1+d/2)\,d}{\pi^{d/2}}\int_0^\infty k^{d-2}\tilde{\chi}_V(k)\mathrm{d}k\int_0^\infty \frac{J_{d/2}^2(kR)}{(kR)^d}\mathrm{d}R. \tag{67}$$

Using the identity

$$\int_0^\infty \frac{J_{d/2}(x)^2}{x^d}\mathrm{d}x = \frac{\Gamma\left(d/2\right)}{2\Gamma\left(d+1/2\right)\Gamma\left((d+1)/2\right)} \tag{68}$$

in (67) yields (64).

For the first three dimensions, equation (64) gives

$$\Sigma_V(\infty) = \begin{cases} \dfrac{1}{2}\displaystyle\int_0^\infty \frac{\tilde{\chi}_V(k)}{k}\mathrm{d}k, & d=1 \\ \dfrac{8}{3\pi^2}\displaystyle\int_0^\infty \tilde{\chi}_V(k)\mathrm{d}k, & d=2 \\ \dfrac{3}{10\pi}\displaystyle\int_0^\infty k\tilde{\chi}_V(k)\mathrm{d}k, & d=3. \end{cases} \tag{69}$$

Referring to the scaling relations (7) and (8), we see that for $d=1$, the integral $\Sigma_V(\infty)$ converges only for hyperuniform media that belong to class I or II. By contrast, it does not converge for $d=1$ for class III hyperuniform media or nonhyperuniform media. For typical nonhyperuniform media and hyperuniform media, $\Sigma_V(\infty)$ converges for any $d \geq 2$. For antihyperuniform media, $\Sigma_V(\infty)$ is nonconvergent if α lies between $-d$ and $2-d$, implying that it is always nonconvergent for $d=1$ and $d=2$, but for $d=3$, it is nonconvergent only if α lies in the open interval $(-3,-1)$. For $d=3$, $\Sigma_V(\infty)$ is convergent for antihyperuniform media if α lies in the open interval $(-1,0)$. Whenever $\Sigma_V(\infty)$ does not converge, we utilize the rate of growth of the integral (62) with L as the order metric.

6. Results

In the ensuing description, we present results for the local variance (as obtained from either (1) or (3)) and its corresponding integral for the 1D, 2D and 3D models discussed in section 4. However, in order to compare different models in any particular space dimension, we fix both the volume fraction ϕ_1 and specific surface s. The latter implies that the characteristic microscopic length scale D is set equal to the inverse of the specific surface, i.e., $D = s^{-1}$. The justification for the use of the specific surface as a simple means to fix length scales for different media was provided by Kim and Torquato [49].

6.1. 1D models

In what follows, we obtain exact closed-form formulas for $\sigma_V^2(R)$ and $\Sigma_v(L)$ for five of the six 1D models considered in this work, except in the case of equilibrium hard rods, which requires numerical quadrature. For a particular model, we express formulas in terms of the characteristic microscopic length scales defined in section 4.

For 1D Debye random media, the local variance is given by

$$\sigma_V^2(R) = \phi_1\phi_2\left(\frac{a}{R}\right) + \frac{\phi_1\phi_2[1-\exp(-2R/a)]}{2}\left(\frac{a}{R}\right)^2. \tag{70}$$

The large-R asymptotic coefficients in distance units a are given by

$$\bar{A}_V = \phi_1\phi_2, \qquad \bar{B}_V = -\frac{\phi_1\phi_2}{2}. \tag{71}$$

The integral of the variance from $R = 0$ to $R = L$ is given by

$$\Sigma_V(L) = \frac{a\phi_1\phi_2}{2}\left[2(\gamma-1) + \frac{a\left(1-\exp(-2L/a)\right)}{L} - 2\mathrm{Ei}\left(-\frac{2L}{a}\right) + \ln(4) + 2\ln\left(\frac{L}{a}\right)\right], \tag{72}$$

where $\gamma = 0.577\,216\ldots$ is the Euler–Mascheroni constant, and $\mathrm{Ei}(x) = -\int_{-x}^{\infty} \mathrm{e}^{-t}\mathrm{d}t/t$ is the exponential integral.

For the 1D random checkerboard, the local variance is given by

$$\sigma_V^2(R) = \begin{cases} \phi_1\phi_2\left[1 - \dfrac{2}{3}\left(\dfrac{R}{a}\right)\right], & R \leqslant a/2 \\ \phi_1\phi_2\left[\dfrac{1}{2}\left(\dfrac{a}{R}\right) - \dfrac{1}{12}\left(\dfrac{a}{R}\right)^2\right], & R \geqslant a/2. \end{cases} \tag{73}$$

The large-R asymptotic coefficients in distance units a are given by

$$\bar{A}_V = \frac{\phi_1\phi_2}{2}, \qquad \bar{B}_V = -\frac{\phi_1\phi_2}{12}. \tag{74}$$

The integral of the variance from $R = 0$ to $R = L$ is given by

$$\Sigma_V(L) = \frac{-\phi_1\phi_2}{12aL}\left[4L^2(L-3a) - \Theta\left(L-\frac{a}{2}\right) \times \left(a^3 - 12aL^2 + 4L^3 + a^2 L\left(3 + \ln(64) + 6\ln\left(\frac{L}{a}\right)\right)\right)\right]. \tag{75}$$

For 1D overlapping rods, the local variance is given by

$$\sigma_V^2(R) = \begin{cases} -\phi_1^2 + \dfrac{2\phi_1}{\eta}\left(\dfrac{a}{R}\right) + \dfrac{2\phi_1(\phi_1^{R/a}-1)}{\eta^2}\left(\dfrac{a}{R}\right)^2, & R \leqslant a \\ 2\phi_1\left(\dfrac{\phi_2}{\eta}-\phi_1\right)\left(\dfrac{a}{R}\right) + \phi_1\left(\phi_1 + \dfrac{2}{\eta}\left(\phi_1 - \dfrac{\phi_2}{\eta}\right)\right)\left(\dfrac{a}{R}\right)^2, & R \geqslant a. \end{cases} \tag{76}$$

The large-R asymptotic coefficients in distance units a are given by

$$\bar{A}_V = 2\phi_1\left(\frac{\phi_2}{\eta}-\phi_1\right), \qquad \bar{B}_V = \phi_1\left(\phi_1 + \frac{2}{\eta}\left(\phi_1 - \frac{\phi_2}{\eta}\right)\right). \tag{77}$$

The integral of the variance from $R = 0$ to $R = L$ is given by

$$\Sigma_V(L) = af(\phi_1) + ag(\phi_1)\frac{(a-L)}{L} + ah(\phi_1)\ln\left(\frac{a}{L}\right), \tag{78}$$

where

$$f(\phi_1) = -\phi_1^2 + \frac{2\phi_1\,\ln(\eta)}{\eta} - \frac{2\phi_1 \mathrm{Ei}(-\eta)}{\eta} + \frac{2(\gamma-1)\phi_1}{\eta} + \frac{2\phi_1}{\eta^2} - \frac{2\phi_1^2}{\eta^2}, \tag{79}$$

$$g(\phi_1) = \frac{\phi_1\,[2\phi_2 - \phi_1(2+\eta)\eta]}{\eta^2}, \tag{80}$$

$$h(\phi_1) = \frac{2\phi_1(\phi_1\eta - \phi_2)}{\eta}. \tag{81}$$

For 1D equilibrium hard rods, the leading order large-R asymptotic coefficient is given exactly by

$$\bar{A}_V = \phi_2(1-\phi_2)^2, \tag{82}$$

which is obtained from (28) and the fact that $S(0) = (1-\phi_2)^2$ [43]. The large-R asymptotic coefficient $\bar{B}_V$ and integral $\Sigma_V(L)$ are computed numerically. However, using the exact low-ϕ_2 asymptotic expansion of $\bar{B}_V$ (which is easily obtained) and the condition that $\bar{B}_V$ must vanish at $\phi_2 = 1$, a fit of the numerical data using a polynomial of degree six (without up to quadratic terms) yields the highly accurate approximation formula in distance units a for $\bar{B}_V$ for all ϕ_2, namely,

$$\bar{B}_V = \frac{-\phi_2}{6}\left(2 - 7\phi_2 + 8\phi_2^2 - 3\phi_2^3\right). \tag{83}$$

For 1D disordered hyperuniform media, the local variance is given by

$$\sigma_V^2(R) = \frac{\phi_1\phi_2 a^2}{4R^2}\left\{1 - [\sin(2R/a) + \cos(2R/a)]\exp(-2R/a)\right\}. \tag{84}$$

The large-R asymptotic coefficients in distance units a are given by

$$\bar{A}_V = 0, \qquad \bar{B}_V = \frac{\phi_1\phi_2}{4}. \tag{85}$$

The integral of the variance over all R is given by

$$\Sigma_V(\infty) = \frac{a\,\pi\phi_1\phi_2}{4}. \tag{86}$$

We consider 1D periodic rods of length $2a = \phi_2 b$ arranged on the sites of the integer lattice $\mathbb{Z}$, where b is the lattice spacing. The local variance was determined analytically in reference [65], but here we present slightly more compact formulas. Specifically, we write the local variance for this periodic medium as follows:

$$\sigma_v^2(R) = \frac{1}{4}\left(G - G^2 - \frac{F}{3}\right)\left(\frac{F}{R}\right)^2, \tag{87}$$

where

$$F = \begin{cases} \min\{\{2R\}, 2a\}, & 2a \leqslant 1 - \{2R\} \\ \min\{1 - \{2R\}, 1 - 2a\}, & 2a \geqslant 1 - \{2R\}, \end{cases} \tag{88}$$

$$G = \begin{cases} \max\{\{2R\}, 2a\}, & 2a \leqslant 1 - \{2R\} \\ \max\{1 - \{2R\}, 1 - 2a\}, & 2a \geqslant 1 - \{2R\}, \end{cases} \tag{89}$$

and $\{x\}$ denotes the fractional part of x.

From relation (87), we can ascertain that the large-R asymptotic coefficients in distance units a are given by

$$\bar{A}_V = 0, \qquad \bar{B}_V = \frac{\phi_1^2}{6}. \tag{90}$$

We also find that the integral of the variance over all R is given by the following infinite sum:

$$\Sigma_V(\infty) = \frac{a}{\pi^2\phi_2}\sum_{n=1}^{\infty}\frac{\sin^2(n\pi\phi_2)}{n^3} \leqslant \frac{a\,\zeta(3)}{\pi^2\phi_2}, \tag{91}$$

where $\zeta(x)$ is the Riemann zeta function. The upper bound on $\Sigma_V(\infty)$ immediately follows by setting the numerator in (91) to its maximal value of unity. The quantity $\Sigma_V(\infty)$ is a function of ϕ_2 that is symmetric about $\phi_2 = 1/2$, where it is achieves its maximal value, and equal to zero at the extreme values of ϕ_2, i.e., $\phi_2 = 0$ and $\phi_2 = 1$. It is noteworthy that when ϕ_2 is a rational number such that $\sin^2(\pi\phi_2)$ is a rational number, the infinite sum can be exactly represented entirely in terms of $\zeta(3) = 1.202\ 056\ 903\ldots$. Specifically, when ϕ_2 equals $1/2, 1/3, 1/4$, and $1/6$, $\Sigma_V(\infty)$ equals $7\zeta(3)/(8\pi^2)$, $13\zeta(3)/(18\pi^2)$, $35\zeta(3)/(64\pi^2)$, $\zeta(3)/(3\pi^2)$, respectively. Whenever $\sin^2(\pi\phi_2)$ is irrational, the infinite sum must be approximated by a finite sum, but the resulting value is highly accurate because (91) converges rapidly.

Table 1 lists closed-form formulas and numeric values of the asymptotic coefficients $\bar{A}_V$ and $\bar{B}_V$ for the 1D models. The 'volume' coefficient $\bar{A}_V$, which measures order at large length scales for nonhyperuniform media, is largest for Debye random media among all models considered and substantially larger for most values of ϕ_2 than $\bar{A}_V$ for overlapping rods, which is the second largest. The coefficient $\bar{A}_V$ for the random checkerboard and equilibrium rods are identical and the smallest among the nonhyperuniform models. We note that when ϕ_2 is sufficiently large, $\bar{B}_V$ for equilibrium hard rods becomes positive (reflecting strong correlations), which indicates that this system becomes more ordered than the random checkerboard, flipping the ranking indicated in table 1. For the hyperuniform models, we see that $\bar{B}_V$ is smaller

Table 1. Comparison of the asymptotic coefficients $\bar{A}_V$ and $\bar{B}_V$ for the 1D models. The microscopic characteristic length scale D is chosen to be s^{-1}, where s is the specific surface.

Model	$\bar{A}_V$	$\bar{B}_V$	$\bar{A}_V(\phi_1 = \frac{1}{2})$	$\bar{B}_V(\phi_1 = \frac{1}{2})$
Debye random media	$2(\phi_1\phi_2)^2$	$-2(\phi_1\phi_2)^3$	0.125 00	−0.031 25
Overlapping rods	$2\phi_1^2(\phi_2 - \phi_1\eta)$	$\phi_1^3(\phi_1\eta^2 + 2\phi_1\eta - 2\phi_2)$	0.076 71	−0.008 33
Equilibrium hard rods	$(\phi_1\phi_2)^2$	$-\frac{\phi_2^3}{6}\left(2 - 7\phi_2 + 8\phi_2^2 - 3\phi_2^3\right)$	0.062 50	−0.002 60
Random checkerboard	$(\phi_1\phi_2)^2$	$-\frac{1}{3}(\phi_1\phi_2)^3$	0.062 50	−0.005 21
Disordered hyperuniform	0	$4(\phi_1\phi_2)^3$	0	0.062 50
Periodic rods	0	$\frac{1}{6}(\phi_1\phi_2)^2$	0	0.010 42

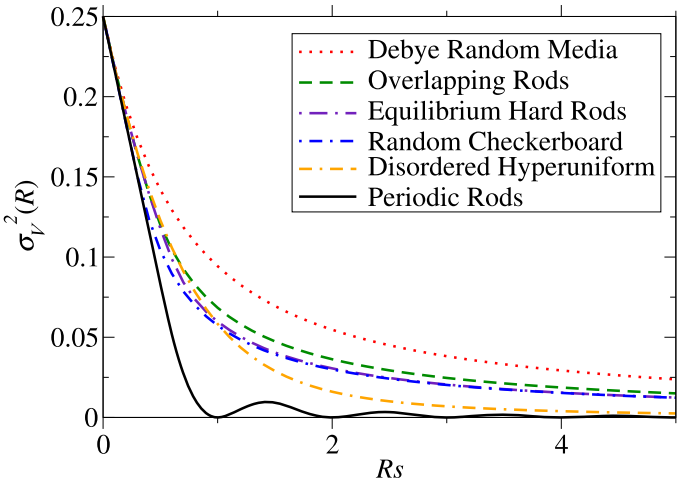

Figure 7. Comparison of the local volume-fraction variance $\sigma_V^2(Rs)$ versus the dimensionless window radius Rs for 1D models at $\phi_2 = 0.5$, where s is the specific surface. For any particular value of R, the lower (higher) the value of $\sigma_V^2(Rs)$, the greater the degree of order (disorder).

for periodic rods than it is for disordered hyperuniform media which is consistent with intuition. In summary, when ranking the degree of order of different nonhyperuniform media with asymptotic coefficients, it is best to use $\bar{A}_V$ as this coefficient weights the dominant term in the large-R asymptotic expansion of the variance for these systems. Analogously, one should use the coefficient $\bar{B}_V$ when ranking order among hyperuniform media.

Figure 7 compares plots of the local volume-fraction variance $\sigma_V^2(Rs)$ versus the dimensionless window radius Rs for 1D models where $\phi_2 = 0.5$. We see that local volume-fraction fluctuations for all window radii are bounded from above by Debye random media and from below by periodic rods. Table 2 provides values of the local volume-fraction variance $\sigma_V^2(Rs)$ for selected values of the dimensionless window radius Rs. For almost all values of Rs, the ranking of the models is in the order indicated in figure 7 and table 1, i.e., Debye random media is the most disordered, whereas periodic rods are the most ordered. It is noteworthy that the ranking ascertained from figure 7 and table 2 is consistent with that predicted by the coefficients $\bar{A}_V$ and $\bar{B}_V$ for the nonhyperuniform and hyperuniform models, respectively. Interestingly, for $Rs \gtrsim 1$, the local variances for equilibrium hard rods and the random checkerboard

Table 2. Comparison of the local volume-fraction variance $\sigma_V^2(Rs)$ for 1D models at $\phi_2 = 0.5$ for selected values of the dimensionless window radius Rs, where s is the specific surface. For any particular value of R, the lower (higher) the value of $\sigma_V^2(Rs)$, the greater the degree of order (disorder). Included in the table is the value of the integral $\Sigma_V(\infty)$.

1D model	$\sigma_V^2(0.3)$	$\sigma_V^2(1)$	$\sigma_V^2(4.5)$	$\sigma_V^2(9.5)$	$\sigma_V^2(50)$	$\sigma_V^2(100)$	$\Sigma_V(\infty)$
Debye random media	0.174 03	0.094 32	0.026 23	0.012 81	0.002 49	0.001 25	$+\infty$
Overlapping rods	0.163 37	0.068 38	0.016 64	0.007 98	0.001 53	0.000 77	$+\infty$
Equilibrium hard rods	0.163 37	0.059 74	0.013 76	0.006 55	0.001 25	0.000 62	$+\infty$
Random checkerboard	0.150 46	0.057 29	0.013 63	0.006 52	0.001 25	0.000 62	$+\infty$
Disordered hyperuniform	0.164 70	0.058 33	0.003 09	0.000 69	0.000 02	0.000 01	0.196 35
Periodic rods	0.150 00	0.000 00	0.001 03	0.000 23	0.000 00	0.000 00	0.106 45

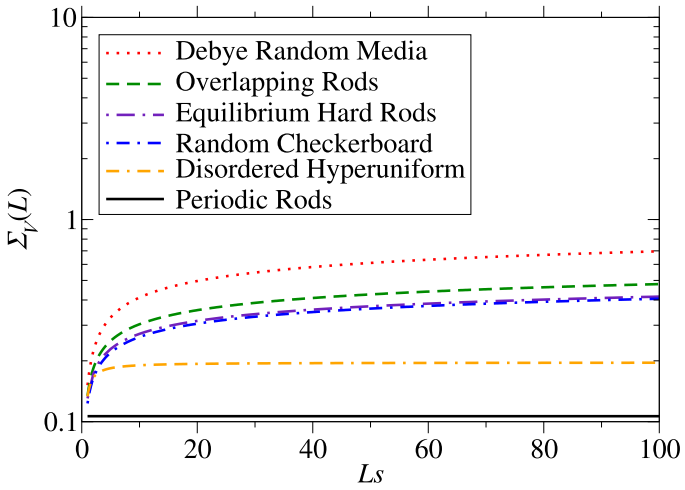

Figure 8. Comparison of the integral of the local volume-fraction variance $\Sigma_V(Ls)$ versus the dimensionless distance Ls for 1D models at $\phi_2 = 0.5$, where s is the specific surface.

are essentially identical. For $Rs \lesssim 1$, the random checkerboard is the second most ordered microstructure due to a greater degree of clustering on the underlying integer lattice at those length scales, which reduces volume-fraction fluctuations relative to those of hard rods. As expected, the disordered hyperuniform model is the second most ordered microstructure for almost all length scales ($Rs \gtrsim 1$). Table 2 also lists the values of $\Sigma_V(\infty)$ for the models. While $\Sigma_V(\infty)$ is divergent for all 1D nonhyperuniform media, for reasons noted above, the magnitude of $\Sigma_V(\infty)$ for the hyperuniform models provides an integral measure over all length scales that is consistent with almost all local values of the variance, except when Rs is very small.

Figure 8 compares plots of the integral of the local volume-fraction variance $\Sigma_V(Ls)$ versus the dimensionless window radius Ls for 1D models where $\phi_2 = 0.5$. The rate of growth of $\Sigma_V(Ls)$ with the dimensionless length Ls for all nonhyperuniform media is consistent with the aforementioned ranking of the 1D models for the local variance indicated in figure 7, tables 1 and 2. Of course, $\Sigma_V(Ls)$ achieves a constant asymptotic value for the hyperuniform models in the limit $Ls \to \infty$.

Table 3. Comparison of the asymptotic coefficients $\bar{A}_V$ and $\bar{B}_V$ for the 2D models at $\phi_2 = 0.4$. The microscopic characteristic length scale D is chosen to be s^{-1}, where s is the specific surface.

Model	$\bar{A}_V$	$\bar{B}_V$
Debye random media	0.272 87	−0.261 96
Overlapping disks	0.078 08	−0.026 79
Random checkerboard	0.070 41	−0.022 44
Equilibrium hard disks	0.03827	−0.002 08
Disordered hyperuniform	0	0.065 49
Stealthy hyperuniform	0	0.011 83
Triangular lattice hexagons	0	0.009 65
Triangular lattice disks	0	0.008 44

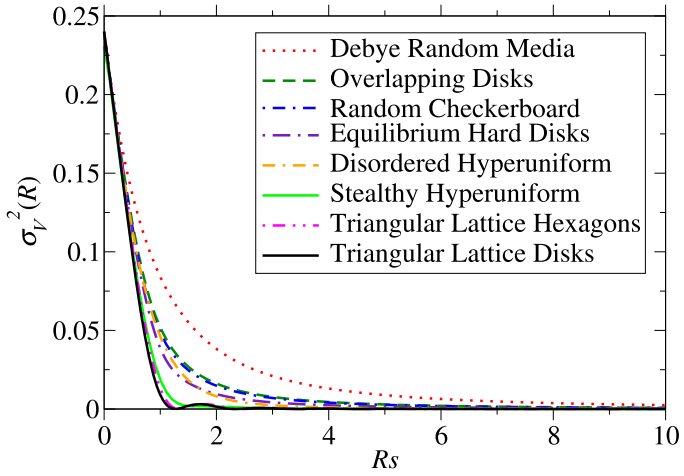

Figure 9. Comparison of the local volume-fraction variance $\sigma_V^2(Rs)$ versus the dimensionless window radius Rs for 2D models at $\phi_2 = 0.4$, where s is the specific surface. For any particular value of R, the lower (higher) the value of $\sigma_V^2(Rs)$, the greater the degree of order (disorder).

6.2. 2D models

We present exact closed-form formulas for $\sigma_V^2(Rs)$ and $\Sigma_V(\infty)$ for Debye random media. For the remaining seven 2D models described in section 4, we compute the same quantities for a volume fraction of phase 2 $\phi_2 = 0.4$, which is chosen because this is nearly the highest value of ϕ_2 consistent with a disordered stealthy hyperuniform packing. Here we also consider stealthy hyperuniform packings, which we did not examine in one dimension. In the case of 2D periodic packings, we study the effect of particle shape on the degree of order by considering both circular disks and hexagons on the sites of the triangular lattice.

For a 2D Debye random medium, the local variance is given by

$$\sigma_V^2(R) = \phi_1\phi_2 \left\{ \left[4I_0(2R/a) - 4L_0(2R/a) + 2\right] \left(\frac{a}{R}\right)^2 + 6\left[-I_1(2R/a) + L_1(2R/a)\right] \left(\frac{a}{R}\right)^3 \right\}, \tag{92}$$

Table 4. Comparison of the local volume-fraction variance $\sigma_V^2(Rs)$ for 2D models at $\phi_2 = 0.4$ for selected values of the dimensionless window radius Rs, where s is the specific surface. For any particular value of R, the lower (higher) the value of $\sigma_V^2(Rs)$, the greater the degree of order (disorder). Included in the table is the value of the integral $\Sigma_V(\infty)$.

2D model	$\sigma_V^2(0.3)$	$\sigma_V^2(1)$	$\sigma_V^2(4.5)$	$\sigma_V^2(9.5)$	$\sigma_V^2(50)$	$\sigma_V^2(100)$	$\Sigma_V(\infty)$
Debye random media	0.169 78	0.084 06	0.010 64	0.002 72	0.000 11	0.000 03	0.307 20
Overlapping disks	0.161 64	0.051 86	0.003 56	0.000 83	0.000 03	0.000 01	0.187 30
Random checkerboard	0.161 00	0.048 38	0.003 23	0.000 75	0.000 03	0.000 01	0.185 09
Equilibrium hard disks	0.231 45	0.038 78	0.001 66	0.000 42	0.000 02	3.733×10^{-6}	0.158 80
Disordered hyperuniform	0.158 31	0.046 16	0.000 71	0.000 08	5.239×10^{-7}	6.549×10^{-8}	0.153 60
Stealthy hyperuniform	0.155 28	0.001 94	0.000 12	0.000 01	9.372×10^{-8}	9.541×10^{-9}	0.118 90
Triangular lattice hexagons	0.156 61	0.013 19	0.000 03	0.000 02	1.351×10^{-7}	6.721×10^{-10}	0.115 23
Triangular lattice disks	0.154 26	0.009 15	0.000 01	3.758×10^{-6}	9.588×10^{-8}	1.480×10^{-8}	0.110 71

where $I_\alpha(x)$ is the modified Bessel function of the first kind of order α, and $L_\alpha(x)$ is the modified Struve function of order α. The large-R asymptotic coefficients in distance units of a are given by

$$\bar{A}_V = 2\phi_1\phi_2, \qquad \bar{B}_V = -\frac{8\phi_1\phi_2}{\pi}. \tag{93}$$

The integral of the variance over all R is given by

$$\Sigma_V(\infty) = \frac{16}{3\pi}. \tag{94}$$

Table 3 lists numeric values of the asymptotic coefficients $\bar{A}_V$ and $\bar{B}_V$ for the 2D models at $\phi_2 = 0.4$. Here, the nonhyperuniform and hyperuniform media are listed in order of decreasing $\bar{A}_V$ and $\bar{B}_V$, respectively, reflecting the ranking of the degree of order in these systems by the asymptotic coefficients. Figure 9 compares plots of the local volume-fraction variance $\sigma_V^2(Rs)$ versus the dimensionless window radius Rs for the 2D models at $\phi_2 = 0.4$. Similar to what was observed in the 1D models, we see that the local volume-fraction variance for the 2D models are bounded from above by Debye random media for all window radii and bounded from below by the triangular lattice of circular disks for most window radii. Table 4 provides values of the local volume-fraction variance $\sigma_V^2(Rs)$ for selected values of the dimensionless window radius Rs. For almost all values of Rs, the ranking of the models is in the order indicated in figure 9 and tables 3 and 4, i.e., Debye random media is the most disordered, down to the triangular lattice of circular disks, which is the most ordered for the reasons noted in section 4.10. While overlapping disks is the second most disordered model (as it is for the 1D models considered), the random checkerboard is more disordered than equilibrium hard disks for almost all length scales ($Rs \gtrsim 1$), reversing the general trend observed for their 1D counterparts (see figure 7 and table 2). This reversal of rank ordering highlights the effect of dimensionality on the degree of order for the same models and occurs for the reasons given in section 4.10, i.e., the spectral density for equilibrium hard disks is lower than that of the random checkerboard for small wavenumbers (see figure 4). The fact that the stealthy packing is the most ordered among the disordered models was also explained in section 4.10. Lastly, we note that the ranking of order via the integrated variance $\Sigma_V(\infty)$ in the rightmost column of table 4 agrees with that given by both the asymptotic coefficients as well as the values of the local variance $\sigma_V^2(Rs)$ for very large (e.g., $Rs > 100$) length scales.

6.3. 3D models

We present exact closed-form formulas for $\sigma_V^2(R)$ and $\Sigma_V(L)$ or $\Sigma_V(\infty)$ for three of the eight 3D models described in section 4: antihyperuniform media, Debye random media, and disordered hyperuniform media. In all other cases, we compute the same quantities for a phase 2 volume fraction $\phi_2 = 0.38$, which is chosen because this is nearly the highest value of ϕ_2 consistent with a disordered stealthy packing. We also consider antihyperuniform media, which was not done in the lower dimensions. In the case of 3D periodic packings of spheres, we study the effect of the lattice on the degree of order by considering both the SC and BCC arrangements.

For the 3D antihyperuniform model defined in section 4, the local variance is given by

Table 5. Comparison of the asymptotic coefficients $\bar{A}_V$ and $\bar{B}_V$ for the 3D models at $\phi_2 = 0.38$. The microscopic characteristic length scale D is chosen to be s^{-1}, where s is the specific surface.

Model	$\bar{A}_V$	$\bar{B}_V$
Antihyperuniform media	—	—
Debye random media	1.183 13	−2.508 71
Random checkerboard	0.158 88	−0.111 46
Overlapping spheres	0.139 94	−0.094 22
Equilibrium hard spheres	0.026 80	0.01765
Disordered hyperuniform	0	0.705 57
Simple cubic	0	0.016 93
Stealthy hyperuniform	0	0.015 39
Body centered cubic	0	0.011 71

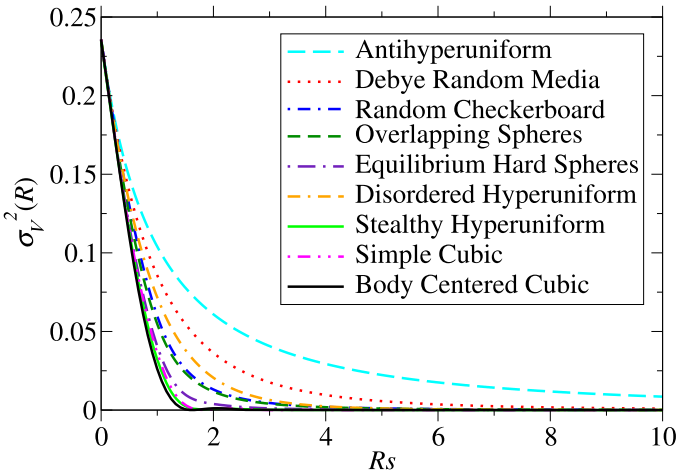

Figure 10. Comparison of the local volume-fraction variance $\sigma_V^2(Rs)$ versus the dimensionless window radius Rs for 3D models at $\phi_2 = 0.38$, where s is the specific surface. For any particular value of R, the lower (higher) the value of $\sigma_V^2(Rs)$, the greater the degree of order (disorder).

$$\sigma_v^2(R) = \frac{9\phi_1\phi_2}{4}\left(\frac{a}{R}\right)^2 + \frac{\phi_1\phi_2}{16}\left[176 - 96\ln\left(\frac{2R}{a}+1\right)\right]\left(\frac{a}{R}\right)^3 + \frac{\phi_1\phi_2}{16}\left[30 - 108\ln\left(\frac{2R}{a}+1\right)\right]\left(\frac{a}{R}\right)^4 - \frac{15\phi_1\phi_2}{8}\left(\frac{a}{R}\right)^5 + \frac{15\phi_1\phi_2}{16}\ln\left(\frac{2R}{a}+1\right)\left(\frac{a}{R}\right)^6. \tag{95}$$

Notice that for large R, the variance has the scaling $\sigma_v^2(R) \sim R^{-2}$, which is clearly slower than window-volume decay (i.e., R^{-3}) obeyed by typical nonhyperuniform media. Thus, the asymptotic coefficients $\bar{A}_V$ and $\bar{B}_V$ do not exist, i.e., they are unbounded. The integral of the

Table 6. Comparison of the local volume-fraction variance $\sigma_V^2(Rs)$ for 3D models at $\phi_2 = 0.38$ for selected values of the dimensionless window radius Rs, where s is the specific surface. For any particular value of R, the lower (higher) the value of $\sigma_V^2(Rs)$, the greater the degree of order (disorder). Included in the table is the value of the integral $\Sigma_V(\infty)$.

Model	$\sigma_V^2(0.3)$	$\sigma_V^2(1)$	$\sigma_V^2(4.5)$	$\sigma_V^2(9.5)$	$\sigma_V^2(50)$	$\sigma_V^2(100)$	$\Sigma_V(\infty)$
Antihyper. media	0.175 38	0.103 96	0.025 45	0.009 21	0.000 57	0.000 16	∞
Debye random media	0.171 04	0.085 67	0.007 31	0.001 08	9.064×10^{-6}	1.158×10^{-6}	0.266 44
Random checkerboard	0.168 13	0.059 82	0.001 47	0.000 17	1.246×10^{-6}	1.568×10^{-7}	0.180 15
Overlapping spheres	0.164 56	0.054 71	0.001 31	0.000 15	1.105×10^{-6}	1.391×10^{-7}	0.171 32
Equil. hard spheres	0.160 98	0.040 70	0.000 32	0.000 03	2.163×10^{-7}	2.695×10^{-8}	0.142 26
Disordered hyper.	0.167 85	0.071 69	0.001 53	0.000 08	1.128×10^{-7}	7.054×10^{-9}	0.199 83
Stealthy hyper.	0.158 74	0.031 97	0.000 03	1.869×10^{-6}	2.492×10^{-9}	1.450×10^{-10}	0.127 95
Simple cubic	0.159 61	0.036 31	7.524×10^{-6}	6.757×10^{-8}	4.653×10^{-10}	2.467×10^{-10}	0.131 76
Body centered cubic	0.159 16	0.026 02	0.000 05	2.320×10^{-7}	1.920×10^{-9}	4.859×10^{-12}	0.123 27

variance from $R = 0$ to $R = L$ is given by

$$\Sigma_V(L) = \frac{6a\phi_1\phi_2}{5} - \frac{9a\phi_1\phi_2}{4}\left(\frac{a}{L}\right) + a\phi_1\phi_2\left[3\,\ln\left(\frac{2L}{a}+1\right) - 4\right]\left(\frac{a}{L}\right)^2 + \frac{9a\phi_1\phi_2}{4}\left[\ln\left(\frac{2L}{a}+1\right) - \frac{1}{6}\right]\left(\frac{a}{L}\right)^3 + \frac{3a\phi_1\phi_2}{8}\left(\frac{a}{L}\right)^4 - \frac{3a\phi_1\phi_2}{16}\,\ln\left(\frac{2L}{a}+1\right)\left(\frac{a}{L}\right)^5. \tag{96}$$

For 3D Debye random media, the local variance is given by

$$\sigma_V^2(R) = \phi_1\phi_2\left\{3\left[2 - 3\,\exp(-2R/a)\right]\left(\frac{a}{R}\right)^3 - \frac{9}{2}\left[3 + 7\,\exp(-2R/a)\right]\left(\frac{a}{R}\right)^4 - 45\,\exp(-2R/a)\left(\frac{a}{R}\right)^5 + \frac{45}{2}\left[1 - \exp(-2R/a)\right]\left(\frac{a}{R}\right)^6\right\}. \tag{97}$$

The large-R asymptotic coefficients in distance units of a are given by

$$\bar{A}_V = 6\phi_1\phi_2, \qquad \bar{B}_V = -\frac{27\phi_1\phi_2}{2}. \tag{98}$$

The integral of the variance over all R is given by

$$\Sigma_V(\infty) = \frac{6\phi_1\phi_2 a}{5}. \tag{99}$$

The local variance of 3D disordered hyperuniform media is given by

$$\sigma_V^2(R) = \phi_1\phi_2\,\exp\left(\frac{-2R}{a}\right)\left\{\left[\frac{27\sqrt{3}}{8}\,\sin\left(\frac{2R}{a\sqrt{3}}\right)\right]\left(\frac{a}{R}\right)^3 + \frac{1}{64}\left[243\,\exp\left(\frac{2R}{a}\right) + 567\sqrt{3}\,\sin\left(\frac{2R}{a\sqrt{3}}\right) + 567\,\cos\left(\frac{2R}{a\sqrt{3}}\right)\right] \times \left(\frac{a}{R}\right)^4 + \frac{1}{64}\left[405\sqrt{3}\,\sin\left(\frac{2R}{a\sqrt{3}}\right) + 1215\,\cos\left(\frac{2R}{a\sqrt{3}}\right)\right]\left(\frac{a}{R}\right)^5 + \frac{1215}{128}\left[\cos\left(\frac{2R}{a\sqrt{3}}\right) - \exp\left(\frac{2R}{a}\right)\right]\left(\frac{a}{R}\right)^6\right\} \tag{100}$$

The large-R asymptotic coefficients in distance units a are given by

$$\bar{A}_V = 0, \qquad \bar{B}_V = \frac{243\phi_1\phi_2}{64}. \tag{101}$$

The integral of the variance over all R is given by

$$\Sigma_V(\infty) = \frac{9\phi_1\phi_2 a}{10}, \tag{102}$$

which, as expected, is smaller than that for 3D Debye random media [cf (99)].

Table 5 provides values of the asymptotic coefficients $\bar{A}_V$ and $\bar{B}_V$ for the 3D models at $\phi_2 = 0.38$. Once again, the nonhyperuniform and hyperuniform media are listed in order of

decreasing $\bar{A}_V$ and $\bar{B}_V$, respectively. Notably, $\bar{B}_V$ ranks the disordered stealthy hyperuniform packing as more ordered than the crystalline SC one. Figure 10 compares plots of the local volume-fraction variance $\sigma_V^2(Rs)$ versus the dimensionless window radius Rs for the 3D models at $\phi_2 = 0.38$. From this plot, we see that local volume-fraction variances in the 3D models are bounded from above by antihyperuniform media for all window radii and bounded from below by BCC lattice of spheres for nearly all window radii. Table 6 provides values of the local volume-fraction variance $\sigma_V^2(Rs)$ for selected values of the dimensionless window radius Rs. For almost all values of Rs, the ranking of the models is in the order indicated in figure 10 and table 6, i.e., the antihyperuniform model is the most disordered, followed by Debye random media, down to the BCC lattice of spheres, which is the most ordered for reasons noted in section 4.10. However, ranking order according to the integrated variance $\Sigma_V(\infty)$ predicts that the disordered (nonstealthy) hyperuniform model lies between Debye random media and the random checkerboard, implying that the hyperuniform medium possesses a higher degree of disorder at short and intermediate length scales which outweighs the high degree of long-range order characteristic of hyperuniform media. Unlike what was observed in the 1D and 2D models, this ranking of order according to $\Sigma_V(\infty)$ contrasts that predicted by both the local variance at large length scales and the asymptotic coefficients $\bar{A}_V$ and $\bar{B}_V$ and can be explained by comparing the relative sizes of the spectral densities for these systems presented in figure 5.

As was observed in the 1D and 2D models, Debye random media is still the most disordered among all of the *typical* disordered nonhyperuniform [cf (9)] models considered here. We also note that, as was the case in 2D, the stealthy packing is the most ordered among the disordered models and the SC lattice packing according to all three order metrics. In both cases, these results occur for reasons provided in section 4.10. Interestingly, the 3D random checkerboard is more disordered than overlapping spheres for all length scales, reversing the ranking of their 2D counterparts (see figure 9 and table 4). Overall, we see that the random checkerboard becomes progressively more disordered relative to the other models as the spatial dimension increases, again, highlighting the effect of dimensionality on the degree of order for a given system. This growing disorder with d in the random checkerboard model can be attributed to a generalized decorrelation principle [23, 66] (see section 7 for more information).

7. Conclusions and discussion

In this work, we have taken initial steps to devise order metrics to characterize the microstructures of disordered and ordered two-phase media across all length scales via the local volume-fraction variance $\sigma_V^2(R)$. By studying a total of 22 two-phase models across the first three space dimensions, including those that span from nonhyperuniform and hyperuniform ones with varying degrees of short- and long-range order, we found that $\sigma_V^2(R)$ as a function of the dimensionless window radius Rs provides a reasonably robust and sensitive order metric across length scales. Additionally, we determined that the asymptotic coefficients $\bar{A}_V$ and $\bar{B}_V$ as well as the integrated volume-fraction variance $\Sigma_V(\infty)$ are similarly effective order metrics. To compare the degree of disorder for different microstructures at a fixed volume fraction and at a specific length scale ℓ, the local volume-fraction variance $\sigma_V^2(\ell)$ should be used. To make such comparisons at larger length scales, the asymptotic coefficients $\bar{A}_V$ or $\bar{B}_V$, for nonhyperuniform or hyperuniform media, respectively, are a reasonable and natural choice. Lastly, for an overall quantification of disorder across all length scales in a system, the integrated variance could be used. Importantly, we recommend the use of all three order metrics when ranking different two-phase media in a particular dimension to ascertain cases in which each of them yield the

same or different rankings. In the latter instance, such discrepancies would imply differences in the degree of order at small, intermediate and/or large length scales for the media.

Interestingly, using all three metrics, Debye random media is the most disordered among all of the typical disordered nonhyperuniform [cf (9)] models examined in this work across all three dimensions. In two and three dimensions, we found that the stealthy disordered hyperuniform sphere packing is the most ordered among all disordered models considered. In dimensions one, two, three, the most ordered microstructures, among all of the ones considered, are packings of identical spheres arranged on the sites of the integer, triangular and BCC lattices, respectively. These lattice packings may be the most ordered across the first three space dimensions for similar reasons given in the related problem of the 'diffusion spreadability' [59], as elaborated below. In a future study, it would be interesting to determine the order of maximally random jammed particle packings [8, 67, 68], which are hyperuniform [8], relative to that of the most ordered packings.

An important lesson learned from our study is that the relative order of any particular d-dimensional model can change with d. For example, going from 1D to 3D, the disordered hyperuniform medium becomes progressively more disordered at small and intermediate length scales (even if more ordered at large length scales), having a volume fraction variance comparable to that of the random checkerboard in 3D for smaller window radii. The random checkerboard also becomes progressively more disordered relative to the other models as the dimension increases. Note that the number of neighbors for a cell in the d-dimensional random checkerboard is given by $3^d - 1$. Therefore, as d increases, the number of potential directions for pair correlations increases exponentially, reducing the overall likelihood of spatial correlations in this model. This specific higher-dimensional behavior is a manifestation of the decorrelation principle [23, 66].

It is important to recognize that the ranking of order/disorder of two-phase microstructures via the local variance at fixed phase volume fraction in any particular dimension depends on the choice of the microscopic characteristic length scale D. We have chosen D to be the inverse of the specific surface because it is broadly applicable and easily determined [49]. An interesting topic for future research is the search and evaluation of a length scale D that is superior to s^{-1} for improving the rank order of two-phase microstructures. An obvious extension of the present work is the formulation of order metrics to n-phase media with $n \geq 3$, which is formally straightforward.

To devise a metric that follows previous considerations for point configurations [8] so that a scalar order metric ψ for two-phase media takes on the value 1 for the most ordered state and 0 for the most disordered state for length scales between L_1 and L_2, a reasonable choice that could be used is the following ratio:

$$\psi = \frac{\min_{\mathcal{C}}\{\Sigma_V(L_2) - \Sigma_V(L_1)\}}{\Sigma_V(L_2) - \Sigma_V(L_1)}, \tag{103}$$

where $\Sigma_V(L)$ is defined in (62) and $\mathcal{C}$ denotes the set of all two-phase media. Since the determination of the minimum is a notoriously difficult task for which there are no proofs, in practice, the minimum is determined from all candidate structures. Finally, we note a relationship between the recently introduced concept of 'spreadability' for time-dependent diffusion in two-phase media [59, 69, 70] and the order metric as measured by $\sigma_V^2(R)$. The spreadability was determined for a subset of the models studied here across dimensions. For this common subset of models, the spreadability at short, intermediate, and long times is roughly proportional to the magnitude of the local variance at small, intermediate, and long length scales, respectively, thus registering the same rankings between these common models. Establishing the precise

reasons for this link between the spreadability and the local variance more rigorously is an outstanding problem for future research.

Acknowledgments

The authors gratefully acknowledge the support of the Air Force Office of Scientific Research Program on Mechanics of Multifunctional Materials and Microsystems under Award No. FA9550-18-1-0514 and the Welch Foundation (Grant No. F-1696). ST thanks the Institute for Advanced Study for their hospitality during his sabbatical leave there.

Data availability statement

All data that support the findings of this study are included within the article (and any supplementary files).

Appendix A. General asymptotic analysis

The local volume-fraction variance $\sigma_V^2(R)$ is generally a function that can be decomposed into a global part that decreases with the window radius R and a local part that oscillates on microscopic length scales about the global contribution. The more general large-R asymptotic formula for the variance for a large class of statistically homogeneous media is given by [24]:

$$\sigma_V^2(R) = A_V(R)\left(\frac{D}{R}\right)^d + B_V(R)\left(\frac{D}{R}\right)^{d+1} + o\left(\frac{D}{R}\right)^{d+1}, \tag{A.1}$$

where

$$A_V(R) = \frac{1}{v_1(D)}\int_{|\mathbf{r}|\leqslant 2R} \chi_V(\mathbf{r})\,\mathrm{d}\mathbf{r} \tag{A.2}$$

$$B_V(R) = -\frac{c(d)}{2Dv_1(D)}\int_{|\mathbf{r}|\leqslant 2R} \chi_V(\mathbf{r})\,|\mathbf{r}|\mathrm{d}\mathbf{r}, \tag{A.3}$$

are R-dependent coefficients. Observe that when the coefficients $A_V(R)$ and $B_V(R)$ converge in the limit $R\to\infty$, they are equal to the constants $\bar{A}_V(R)$ and $\bar{B}_V(R)$, defined by (26) and (27), respectively. The more general asymptotic analysis has been applied to yield the scaling laws for class II and class III hyperuniform media indicated in relation (8) [15, 24].

In cases when two-phase media are generated via simulations, it is advantageous to estimate the coefficients $\bar{A}_V$ and $\bar{B}_V$ by using the cumulative moving average, as defined in reference [24], namely,

$$\bar{A}_V \equiv \lim_{L\to\infty}\frac{1}{L}\int_0^L \bar{A}_V(R)\mathrm{d}R, \tag{A.4}$$

$$\bar{B}_V \equiv \lim_{L\to\infty}\frac{1}{L}\int_0^L \bar{B}_V(R)\mathrm{d}R. \tag{A.5}$$

ORCID iDs

Salvatore Torquato https://orcid.org/0000-0003-4614-335X

References

[1] Christensen R M 1979 *Mechanics of Composite Materials* (New York: Wiley)
[2] Torquato S 2002 *Random Heterogeneous Materials: Microstructure and Macroscopic Properties* (Berlin: Springer)
[3] Milton G W 2002 *The Theory of Composites* (Cambridge: Cambridge University Press)
[4] Sahimi M 2003 *Heterogeneous Materials I: Linear Transport and Optical Properties* (Berlin: Springer)
[5] Buryachenko V A 2007 *Micromechanics of Heterogeneous Materials* (Berlin: Springer)
[6] Ghanbarian B, Esmaeilpour M, Ziff R M and Sahimi M 2021 Effect of pore-scale heterogeneity on scale-dependent permeability: pore-network simulation and finite-size scaling analysis *Water Resour. Res.* **57** e2021WR030664
[7] Klatt M A, Ziff R M and Torquato S 2021 Critical pore radius and transport properties of disordered hard-and overlapping-sphere models *Phys. Rev.* E **104** 014127
[8] Torquato S 2018 Perspective: basic understanding of condensed phases of matter via packing models *J. Chem. Phys.* **149** 020901
[9] Yu S, Qiu C W, Chong Y, Torquato S and Park N 2021 Engineered disorder in photonics *Nat. Rev. Mater.* **6** 226–43
[10] Li X, Zhang Y, Zhao H, Burkhart C, Brinson L C and Chen W 2018 A transfer learning approach for microstructure reconstruction and structure-property predictions *Sci. Rep.* **8** 1–13
[11] Carleo G, Cirac I, Cranmer K, Daudet L, Schuld M, Tishby N, Vogt-Maranto L and Zdeborová L 2019 Machine learning and the physical sciences *Rev. Mod. Phys.* **91** 045002
[12] Röding M, Ma Z and Torquato S 2020 Predicting permeability via statistical learning on higher-order microstructural information *Sci. Rep.* **10** 1–17
[13] Bayer B E 1964 Relation between granularity and density for a random-dot model *J. Opt. Soc. Am.* **54** 1485–90
[14] Lu B and Torquato S 1990 Photographic granularity: mathematical formulation and effect of impenetrability of grains *J. Opt. Soc. Am.* A **7** 717–24
[15] Torquato S 2020 Predicting transport characteristics of hyperuniform porous media via rigorous microstructure-property relations *Adv. Water Resour.* **140** 103565
[16] Fishman R S, Kurtze D A and Bierwagen G P 1992 The effects of density fluctuations in organic coatings *J. Appl. Phys.* **72** 3116–24
[17] Botsis J, Beldica C and Zhao D 1994 On strength scaling of composites with long aligned fibres *Int. J. Fract.* **68** 375–84
[18] Keller J B 1964 Stochastic equations and wave propagation in random media *Proc. Symp. Appl. Math.* **16** 145
[19] Kim J and Torquato S 2020 Multifunctional composites for elastic and electromagnetic wave propagation *Proc. Natl Acad. Sci. USA* **117** 8764–74
[20] Dal Negro L 2021 *Waves in Complex Media: Fundamentals and Device Applications* (Cambridge: Cambridge University Press)
[21] Lu B and Torquato S 1990 Local volume fraction fluctuations in heterogeneous media *J. Chem. Phys.* **93** 3452–9
[22] Zachary C E and Torquato S 2009 Hyperuniformity in point patterns and two-phase random heterogeneous media *J. Stat. Mech.* P12015
[23] Torquato S and Stillinger F H 2006 New conjectural lower bounds on the optimal density of sphere packings *Exp. Math.* **15** 307–31
[24] Torquato S 2018 Hyperuniform states of matter *Phys. Rep.* **745** 1–95
[25] Torquato S and Stillinger F H 2003 Local density fluctuations, hyperuniform systems, and order metrics *Phys. Rev.* E **68** 041113
[26] Debye P, Anderson H R and Brumberger H 1957 Scattering by an inhomogeneous solid: II. The correlation function and its application *J. Appl. Phys.* **28** 679–83

[27] Florescu M, Torquato S and Steinhardt P J 2009 Designer disordered materials with large, complete photonic band gaps *Proc. Natl Acad. Sci. USA* **106** 20658–63
[28] Degl'Innocenti R *et al* 2016 Hyperuniform disordered terahertz quantum cascade laser *Sci. Rep.* **6** 19325
[29] Froufe-Pérez L S, Engel M, Sáenz J J and Scheffold F 2017 Band gap formation and Anderson localization in disordered photonic materials with structural correlations *Proc. Natl Acad. Sci. USA* **114** 9570–4
[30] Bigourdan F, Pierrat R and Carminati R 2019 Enhanced absorption of waves in stealth hyperuniform disordered media *Opt. Express* **27** 8666–82
[31] Gorsky S, Britton W A, Chen Y, Montaner J, Lenef A, Raukas M and Dal Negro L 2019 Engineered hyperuniformity for directional light extraction *APL Photon.* **4** 110801
[32] Lei Q-L and Ni R 2019 Hydrodynamics of random-organizing hyperuniform fluids *Proc. Natl Acad. Sci. USA* **116** 22983–9
[33] Sheremet A, Pierrat R and Carminati R 2020 Absorption of scalar waves in correlated disordered media and its maximization using stealth hyperuniformity *Phys. Rev.* A **101** 053829
[34] Zheng Y *et al* 2020 Disordered hyperuniformity in two-dimensional amorphous silica *Sci. Adv.* **6** eaba0826
[35] Christogeorgos O, Zhang H, Cheng Q and Hao Y 2021 Extraordinary directive emission and scanning from an array of radiation sources with hyperuniform disorder *Phys. Rev. Appl.* **15** 014062
[36] Chen D, Zheng Y, Liu L, Zhang G, Chen M, Jiao Y and Zhuang H 2021 Stone–wales defects preserve hyperuniformity in amorphous two-dimensional networks *Proc. Natl Acad. Sci.* **118** e2016862118
[37] Nizam Ü S *et al* 2021 Dynamic evolution of hyperuniformity in a driven dissipative colloidal system *J. Phys.: Condens. Matter* **33** 304002
[38] Torquato S and Kim J 2021 Nonlocal effective electromagnetic wave characteristics of composite media: beyond the quasistatic regime *Phys. Rev.* X **11** 021002
[39] Zhang H, Cheng Q, Chu H, Christogeorgos O, Wu W and Hao Y 2021 Hyperuniform disordered distribution metasurface for scattering reduction *Appl. Phys. Lett.* **118** 101601
[40] Duerinckx M and Gloria A 2022 Sedimentation of random suspensions and the effect of hyperuniformity *Ann. PDE* **8** 1–66
[41] Tavakoli N *et al* 2022 Over 65% sunlight absorption in a 1 μm si slab with hyperuniform texture *ACS Photon.* **9** 1206–17
[42] Torquato S 2016 Disordered hyperuniform heterogeneous materials *J. Phys.: Condens. Matter* **28** 414012
[43] Torquato S 2021 Structural characterization of many-particle systems on approach to hyperuniform states *Phys. Rev.* E **103** 052126
[44] Stanley H E 1987 *Introduction to Phase Transitions and Critical Phenomena* (Oxford: Oxford University Press)
[45] Binney J J, Dowrick N J, Fisher A J and Newman M E J 1992 *The Theory of Critical Phenomena: An Introduction to the Renormalization Group* (Oxford: Oxford University Press)
[46] Mandelbrot B B 1982 *The Fractal Geometry of Nature* (San Francisco, CA: Freeman)
[47] Torquato S, Kim J and Klatt M A 2021 Local number fluctuations in hyperuniform and nonhyperuniform systems: higher-order moments and distribution functions *Phys. Rev.* X **11** 021028
[48] Oğuz E C, Socolar J E S, Steinhardt P J and Torquato S 2019 Hyperuniformity and anti-hyperuniformity in one-dimensional substitution tilings *Acta Crystallogr.* A **75** 3–13
[49] Kim J and Torquato S 2021 Characterizing the hyperuniformity of ordered and disordered two-phase media *Phys. Rev.* E **103** 012123
[50] Chiu S N, Stoyan D, Kendall W S and Mecke J 2013 *Stochastic Geometry and its Applications* 3rd edn (New York: Wiley)
[51] Debye P and Bueche A M 1949 Scattering by an inhomogeneous solid *J. Appl. Phys.* **20** 518–25
[52] Koch K, Ohser J and Schladitz K 2003 Spectral theory for random closed sets and estimating the covariance via frequency space *Adv. Appl. Probab.* **35** 603–13
[53] Gel'fand I and Vilenkin N Y 1964 *Applications of Harmonic Analysis* (New York: Academic)
[54] Zhang G, Stillinger F H and Torquato S 2016 Transport, geometrical, and topological properties of stealthy disordered hyperuniform two-phase systems *J. Chem. Phys.* **145** 244109
[55] Chen D and Torquato S 2018 Designing disordered hyperuniform two-phase materials with novel physical properties *Acta Mater.* **142** 152–61

[56] Hansen J P and McDonald I R 1986 *Theory of Simple Liquids* (New York: Academic)
[57] Percus J 1964 Pair distribution function in classical statistical mechanics *The Equilibrium Theory of Classical Fluids* ed H L Frisch and J L Lebowitz (New York: Benjamin)
[58] Zernike F and Prins J A 1927 Die Beugung von röntgenstrahlen in flüssigkeiten als effekt der molekülanordnung *Z. Phys.* **41** 184–94
[59] Torquato S 2021 Diffusion spreadability as a probe of the microstructure of complex media across length scales *Phys. Rev.* E **104** 054102
[60] Uche O U, Stillinger F H and Torquato S 2004 Constraints on collective density variables: two dimensions *Phys. Rev.* E **70** 046122
[61] Zhang G, Stillinger F and Torquato S 2015 Ground states of stealthy hyperuniform potentials: I. Entropically favored configurations *Phys. Rev.* E **92** 022119
[62] Zhou W, Cheng Z, Zhu B, Sun X and Tsang H K 2016 Hyperuniform disordered network polarizers *IEEE J. Sel. Top. Quantum Electron.* **22** 288–94
[63] Ma Z and Torquato S 2020 Generation and structural characterization of Debye random media *Phys. Rev.* E **102** 043310
[64] Skolnick M and Torquato S 2021 Understanding degeneracy of two-point correlation functions via Debye random media *Phys. Rev.* E **104** 045306
[65] Quintanilla J and Torquato S 1999 Local volume fraction fluctuations in periodic heterogeneous media *J. Chem. Phys.* **110** 3215–9
[66] Torquato S, Uche O U and Stillinger F H 2006 Random sequential addition of hard spheres in high Euclidean dimensions *Phys. Rev.* E **74** 061308
[67] Jiao Y, Stillinger F H and Torquato S 2010 Distinctive features arising in maximally random jammed packings of superballs *Phys. Rev.* E **81** 041304
[68] Ziff R M and Torquato S 2017 Percolation of disordered jammed sphere packings *J. Phys. A: Math. Theor.* **50** 085001
[69] Maher C E, Stillinger F H and Torquato S 2022 Characterization of void space, large-scale structure, and transport properties of maximally random jammed packings of superballs *Phys. Rev. Mater.* **6** 025603
[70] Wang H and Torquato S 2022 Dynamic measure of hyperuniformity and nonhyperuniformity in heterogeneous media via the diffusion spreadability *Phys. Rev. Appl.* **17** 034022